Department of Technical Physics
Faculty of Information Technology
Helsinki University of Technology
FIN-02150 Espoo, Finland

Electromagnetic Theory of Diffractive Optics

Eero Noponen

Dissertation for the degree of Doctor of Technology to be presented with due permission for public examination and debate in Auditorium F1 at Helsinki University of Technology (Espoo, Finland) on the 15th of April, 1994, at 12 o'clock noon.

Espoo 1994

ISBN 951-22-2026-1
VTT OFFSETPAINO, ESPOO 1994

Preface

I have very much enjoyed my participation in the optics group at the Materials Physics Laboratory during the last five years. The fruitful and challenging atmosphere has made my work exceedingly pleasant, for which I give my thanks the whole (past and present) laboratory personnel. In particular, I wish to express my gratitude to Professor Eero Byckling, director of the Materials Physics Laboratory, for his continuous support throughout my work. I would also like to thank him and Professor (acting) Matti Kaivola for providing me with excellent laboratory facilities and favorable working conditions.

To Dr. Jari Turunen I am deeply indebted for his skillful and enthusiastic guidance through the jungle of diffractive optics and for his countless beneficial ideas and views. I owe very special thanks to Dr. Antti Vasara who initiated the research on rigorous diffraction theory and supervised my first steps in this field, not to forget his major contribution to the two earliest papers selected in this thesis. I am also thankful to my other co-authors: Dr. Mohammad R. Taghizadeh and Dr. J. Michael Miller (Heriot-Watt University, UK). In addition, I am much obliged to Mr. Jan Westerholm for the numerous valuable comments and suggestions concerning the manuscript as well as to Dr. Ari T. Friberg, Dr. Eero Tervonen, Mr. Jyrki Saarinen, and Mr. Juhani Huttunen for the rewarding collaboration.

Personal grants from the Emil Aaltonen Foundation, the Jenny and Antti Wihuri Foundation, the Alfred Kordelin Foundation, and the Heikki and Hilma Honkanen Foundation are gratefully acknowledged.

Finally, I wish to express my appreciation for the encouragement and support provided by my family.

Espoo, March 1994
Eero Noponen

List of Publications

This thesis is a review of the author's work in the field of electromagnetic diffraction analysis of diffractive optics. It consists of an overview and the following selection of the author's publications in this field.

I E. Noponen, A. Vasara, J. Turunen, J. M. Miller, and M. R. Taghizadeh, "Synthetic diffractive optics in the resonance domain", *Journal of the Optical Society of America A* **9**, 1206–1213 (1992).

II E. Noponen and J. Turunen, "Eigenmode method for electromagnetic synthesis of diffractive elements with three-dimensional profiles", *Report TKK-F-A726* (1994).

III E. Noponen, J. Turunen, and A. Vasara, "Parametric optimization of multilevel diffractive optical elements by electromagnetic theory", *Applied Optics* **31**, 5910–5912 (1992).

IV E. Noponen, J. Turunen, and A. Vasara, "Electromagnetic theory and design of diffractive-lens arrays", *Journal of the Optical Society of America A* **10**, 434–443 (1993).

V E. Noponen and J. Turunen, "Electromagnetic theory of Talbot imaging", *Optics Communications* **98**, 132–140 (1993).

VI E. Noponen and J. Turunen, "Binary high-frequency-carrier diffractive optical elements: electromagnetic theory", *Journal of the Optical Society of America A* **11**, No. 3 (1994, in press).

Throughout the overview, these papers will be referred to by Roman numerals.

Author's Contribution

The studies reported in this dissertation are the result of group work that has been carried out at the Materials Physics Laboratory of Helsinki University of Technology during the years 1991 – 1993.

The author has had an active role in developing the theories and the techniques reported in Papers I–VI. In particular, he has formulated and implemented all the numerical algorithms and carried out all the numerical calculations. The author also initiated the work that lead to Paper II.

The author has actively participated in the writing of Papers I and III–V. Paper II and the basis of Paper VI were written by him.

Contents

1 Introduction

An intuitive concept of light and its properties is the rectilinear propagation. This model known as ray optics or geometrical optics was found incomplete in the 17th century, when light transmitted through a small aperture was observed to form a spot with smooth boundaries extending into the geometrical shadow of the screen. This phenomenon called diffraction was defined by Sommerfeld as *any deviation of light rays from rectilinear paths which can not be interpreted as reflection or refraction*, and was explained as a consequence of the wave nature of light.

The evolution of the wave diffraction theory was initiated by Huygens in 1678, was contributed to later by Fresnel and Kirchhoff, and was reformulated by Sommerfeld and Rayleigh at the end of the 19th century. These theories treat the propagation of light as a scalar phenomenon and thus neglect its electromagnetic nature: the electromagnetic field must be characterized by its two components, the electric and the magnetic field, which are coupled by Maxwell's equations. In the scalar approach we consider only one transverse component of the field; this approximation is valid, however, if the diffracting object is large compared with the wavelength of light, if the observation distance is sufficiently large, and if the angles involved are small enough to guarantee that the axial field components can be neglected. Widely used approaches include the so-called Fresnel and Fraunhofer approximations [1], which describe the diffraction patterns in the Fresnel region and in the far field of the aperture, respectively.

Although diffraction was originally considered merely a limitation to the performance of optical systems, the use of the phenomenon to advantage has been known for two centuries in the form of diffraction gratings [2–4], elements that periodically modulate the incident wave-front. Their particular significance lies in the characteristics of the diffracted field: an ideal grating generates a set of waves called diffraction orders that propagate into discrete directions. The diffraction angles θ_m (for a reflection-type grating) are given by the well-known grating equation

$$\sin\theta_m = \sin\theta + m\lambda/d \tag{1}$$

in terms of the angle of incidence θ, the wavelength of light λ, and the grating period d, whereas the amplitudes of the diffraction orders are determined by the structure of the periodic modulation. The use of diffraction gratings in spectroscopic applications is motivated by their wavelength selectivity and by their capability to decompose the incident light into a spectrum.

In 1902, Wood [5] discovered abrupt variations of the diffraction efficiency with wavelength for a grating illuminated by a continuous-spectrum light source, which could not be explained using scalar diffraction theories. This effect, the so-called Wood (or Rayleigh-Wood) anomaly [2, 3], originates from the passing-off of a higher diffraction order propagating at the grazing angle, i.e., along the surface of the grating. Another type of anomaly are the so-called resonance anomalies, such as the plasmon anomalies of metallic gratings and the anomalies of dielectric coated gratings, which are due to the excitation of leaky waves or surface waves [6, 7]. Common to these anomalous effects is that they are highly polarization dependent, and the full electromagnetic diffraction theory has to be applied to predict their qualitative and quantitative form [7, 8]. The Rayleigh-Wood and the resonance anomalies are the basis of many well-known phenomena such as the coupling of a laser beam into and out of integrated optics waveguides using a grating coupler [9], the total absorption of light by metallic gratings [10, 11], and, as a recently introduced topic, bandpass filtering using guided-mode resonances in planar dielectric waveguide gratings [12, 13].

To explain the newly observed resonance phenomena Lord Rayleigh made the first attempt to solve the electromagnetic problem of gratings in 1907 [2]. He suggested that the field may be expressed as a simple series expansion both outside the modulated region and inside the grooves of the grating. The Rayleigh expansion is still used to describe the propagation of the electromagnetic field outside the grating, but the latter assumption was found numerically unsatisfactory in certain cases after over half a century. In addition to the question of anomalies, the demand for electromagnetic analysis arose with the advance of the fabrication technology of ruled and holographic gratings, as groove spacings comparable to the wavelength of light become commonplace. Scalar theories fail for such gratings that are operating in what is called the resonance domain. A large number of rigorous vector theories have been presented since 1960's, the majority of which can be classified as integral, differential, or modal formalisms [4, 14].

The progress of diffractive optics has been characterized by remarkable topics such as the Talbot effect [15], the Fresnel lens [16], and optical holography [17, 18]. A significant step was taken as well in the late 1960's, as the development of powerful computers allowed the alternative approach of synthesizing a diffractive element that produces the desired wave-front. Because of the strong historical impact of optical holography, such diffractive elements that are designed and fabricated with the help of a computer are traditionally called computer-generated holograms, synthetic holograms, or digital holograms [19–23]. In this work, however, we try to use a more

accurate terminology that is based, e.g., on the structure of the element.

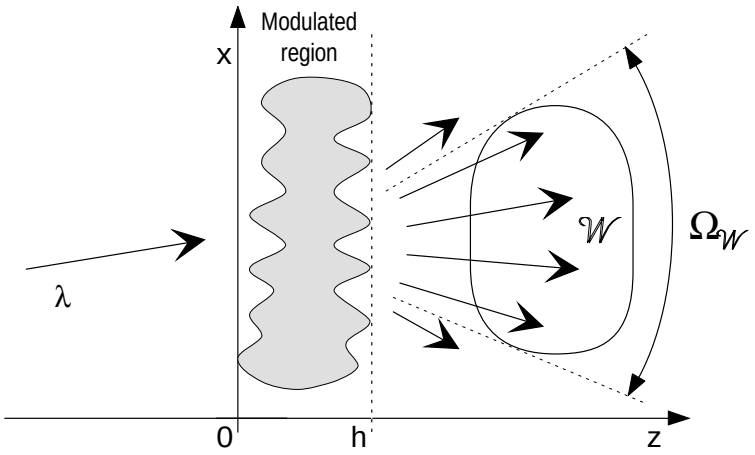

Figure 1: Illustration of the synthesis problem in diffractive optics.

The basic synthesis problem of diffractive optics is illustrated in Fig. 1: the modulated region (scatterer) converts the incident wave into a diffracted wave that has some specified properties in the region $\mathcal{W}$ that we call the signal window. The problem is now to determine the structure of the scatterer that satisfies the constraints given above or at least approximates the desired response. Typically a large number of solutions to the constrained synthesis problem exist, and the choice among them may be based, e.g., on the proportion of the incident power concentrated in $\mathcal{W}$ (the diffraction efficiency).

Depending on the angles involved in the geometry of the diffraction problem, diffractive optics may be divided into paraxial and nonparaxial domains [24]. In the paraxial domain the angular extent $\Omega_{\mathcal{W}}$ of the signal window, the central diffraction angle Ω_C, and the incident angle θ are small, i.e., $\sin\Omega_{\mathcal{W}} \approx \Omega_{\mathcal{W}}$, $\sin\Omega_C \approx \Omega_C$, and $\sin\theta \approx \theta$. The nonparaxial domain is divided further into transitional and resonance domains. Of these two, the transitional domain is still the least explored, although some preliminary investigations have been made [25]. The resonance domain, in which the signal covers essentially the whole halfspace ($\Omega_{\mathcal{W}} \lesssim \pi$), includes gratings for high-resolution spectroscopy as well as novel high-efficiency beam-splitter elements (Papers I and II). On the other hand, the strong polarization effects associated with the subwavelength structures, e.g., gratings with a period below the wavelength of light, have been utilized to realize antireflection surfaces [26–29] and quarter-wave plates [30, 31]. Furthermore, subwavelength structures can be used to modulate the local effective refractive index of the diffractive optical element and to realize graded-index-type elements that, e.g., act like blazed gratings [32–35].

This work covers the electromagnetic analysis and the synthesis of several types of diffractive element. The present summary is a review of Papers I–VI; some theory and results not contained in these papers are also included. The fundamentals of the electromagnetic theory for two-dimensional profiles is presented in Chapter 2, where the numerical algorithm employed in Papers I and III–VI is also described. In addition, some other popular methods are briefly reviewed. The three-dimensional extension of our method is presented in Paper II.

The results of the electromagnetic analysis are divided into three categories: Fourier-type, Fresnel-type, and high-frequency-carrier elements. The analysis of paraxial scalar designs for binary [36] and multilevel [37] array illuminators in the nonparaxial domain is presented in Chapter 3. The numerous possibilities of synthesizing resonance-domain coupler elements (Papers I and II) are then discussed and a selection of optimization results is presented. Chapter 4 deals with Fresnel-domain diffractive elements. As an example, the performance of diffractive-lens arrays is evaluated and enhanced by a rigorous optimization of the local groove structures (Papers III and IV). The Talbot effect and the self-imaging of electromagnetic fields is also investigated (Paper V). The use of binary high-frequency-carrier gratings to realize diffractive elements is considered in Chapter 5, where array illuminators are constructed through pulse-frequency and pulse-width modulation of the carrier grating. Finally, in Chapter 6, the main results are summarized and some future prospects are outlined.

2 Electromagnetic diffraction analysis

The refractive index distribution $n(\mathbf{r})$ of a diffraction grating may in general be periodic in either one or two dimensions and arbitrary in the third dimension (depth). In the case of gratings with two-dimensional periodicity, the so-called crossed gratings, the electromagnetic field vectors $\mathbf{E}$ and $\mathbf{H}$ must be treated simultaneously because of their coupling through Maxwell's equations. A number of methods have been developed for the diffraction analysis of crossed gratings [38–44], including our approach presented in Paper II. However, in this section we restrict our analysis to the simpler case of gratings that are periodic in only one direction, for which the general diffraction problem can be solved by considering independently two scalar problems that correspond to the fundamental states of polarization.

2.1 Electromagnetic theory

In the general case the electric and the magnetic field have a nonvanishing component along all coordinate axes. However, the general linearly polarized case can always be divided into two mutually independent fundamental polarization modes: in TE or transverse electric polarization the $\mathbf{E}$ vector is perpendicular to the plane of incidence, whereas in TM or transverse magnetic polarization the same condition holds for the $\mathbf{H}$ vector [14]. Once the transverse field component is known, the other field vector that lies in the plane of incidence is obtained from Maxwell's equations.

Consider the geometry illustrated in Fig. 2, in which two parallel planes at $z = 0$ and $z = h$ divide the space into three regions labeled I, II, and III. Region I ($z < 0$) is occupied by a homogeneous dielectric medium with a real-valued refractive index n_0, whereas the material in region III ($z > h$) with refractive index n_3 may be either dielectric or metallic; in the latter case the material is conductive, and n_3 is complex valued. The permittivity distribution in the intermediate region II ($0 < z < h$) is periodically modulated in the x direction (period d) but is invariant in the y direction. The permittivity may therefore be written as a Fourier series expansion

$$\epsilon_{\mathrm{II}}(\mathbf{r}) = \epsilon_0 \epsilon_{\mathrm{r}}(x, z) = \epsilon_0 \sum_{p=-\infty}^{\infty} \varepsilon_p(z) \exp(i 2\pi p x/d). \tag{2}$$

A unit-amplitude monochromatic plane wave with vacuum wavelength λ is assumed incident from region I at an angle θ relative to the z axis. In the case of conical

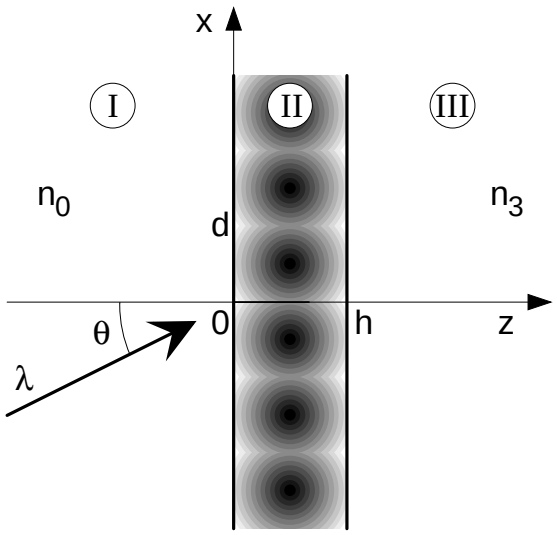

Figure 2: Geometry for diffraction of a plane wave by a grating periodic in one dimension.

incidence [4], the wave vector has a nonzero y component, but we assume here for simplicity that the wave vector lies in the xz plane. Suppressing the common time dependence $\exp(-i\omega t)$, the incident wave may thus be expressed in the form

$$U_0(x,z) = \exp\left[in_0 k(x\sin\theta + z\cos\theta)\right], \tag{3}$$

where $k = 2\pi/\lambda$ is the wave number in vacuum, and U_0 stands for E_y and H_y in TE and TM polarization, respectively.

In the regions I and III with constant refractive index, wave propagation is described by the Helmholtz equation $(\nabla^2 + n^2k^2)U = 0$, where $n = n_0$ or $n = n_3$. The simplest general solutions are plane waves, of which only a discrete set is allowed for a grating. The diffracted field in regions I and III may be expressed in the form of the so-called Rayleigh expansions [2, 14]

$$U_{\mathrm{R}}(x,z) = \sum_{m=-\infty}^{\infty} R_m \exp\left[i(\alpha_m x - r_m z)\right] \tag{4}$$

and

$$U_{\mathrm{T}}(x,z) = \sum_{m=-\infty}^{\infty} T_m \exp\left\{i[\alpha_m x + t_m(z-h)]\right\}, \tag{5}$$

where the coefficients R_m and T_m represent the complex amplitudes of the reflected and the transmitted diffraction orders, respectively;

$$\alpha_m = n_0 k\sin\theta + 2\pi m/d, \tag{6}$$

$$r_m^2 = (n_0 k)^2 - \alpha_m^2, \tag{7}$$

and

$$t_m^2 = (n_3 k)^2 - \alpha_m^2. \tag{8}$$

The signs for r_m and t_m are chosen such that $\mathrm{Re}\{r_m\} + \mathrm{Im}\{r_m\} \geq 0$ and $\mathrm{Re}\{t_m\} + \mathrm{Im}\{t_m\} \geq 0$.

Diffraction orders with real-valued r_m and t_m correspond to plane waves propagating in the regions I and III, respectively, or homogeneous waves. These form the two finite sets $\mathcal{R} = \{m \mid r_m \text{ real}\}$ and $\mathcal{T} = \{m \mid t_m \text{ real}\}$. The propagation angles ϕ_m and θ_m of the reflected and the transmitted diffraction orders are obtained from

$$n_0 \sin\phi_m = n_0 \sin\theta + m\lambda/d \tag{9}$$

and

$$n_3 \sin\theta_m = n_0 \sin\theta + m\lambda/d, \tag{10}$$

respectively. The relative intensities or the efficiencies of the propagating diffraction orders are obtained by calculating the z component of the time-averaged Poynting vector, and they are given by

$$\eta_m = \mathrm{Re}\left\{\frac{r_m}{r_0}\right\} |R_m|^2 \tag{11}$$

and

$$\eta_m = \mathrm{Re}\left\{C\frac{t_m}{r_0}\right\} |T_m|^2 \tag{12}$$

for the reflected and the transmitted diffraction orders, respectively; here $C = 1$ for TE polarization and $C = (n_0/n_3)^2$ for TM polarization. Diffraction orders with imaginary or complex-valued r_m and t_m, called evanescent or inhomogeneous waves, decay exponentially in the medium outside the grating. Propagating orders only are observable in the far field.

In TE polarization $\mathbf{E}(\mathbf{r}) = E_y(x,z)\,\hat{\mathbf{y}}$, and the electric field inside the modulated region II can be shown to satisfy the Helmholtz equation (in a nonmagnetic medium)

$$\left[\frac{\partial^2}{\partial x^2} + \frac{\partial^2}{\partial z^2} + k^2\epsilon_{\mathrm{r}}(x,z)\right] E_y(x,z) = 0. \tag{13}$$

The equation for the y component of the electric field provides the complete solution of the problem, because the lack of x and z dependency in the incident wave implies the

same also for the diffracted field. On the other hand, in TM polarization the magnetic field $\mathbf{H}(\mathbf{r}) = H_y(x,z)\,\hat{\mathbf{y}}$ can be solved from

$$\frac{\partial}{\partial x}\left[\frac{1}{\epsilon_{\mathrm{r}}(x,z)}\frac{\partial H_y(x,z)}{\partial x}\right] + \frac{\partial}{\partial z}\left[\frac{1}{\epsilon_{\mathrm{r}}(x,z)}\frac{\partial H_y(x,z)}{\partial z}\right] + k^2 H_y(x,z) = 0. \qquad (14)$$

Equations (13) and (14) give the general expressions for the electric and the magnetic field in all regions; Rayleigh expansions hold in regions I and III, whereas in region II an expansion specific to each method of solution and grating type has to be found. These expressions contain unknown coefficients, such as R_m and T_m, whose numerical values are determined by the continuity conditions across the boundaries between the regions: Maxwell's equations imply the continuity of the tangential components of $\mathbf{E}$ and $\mathbf{H}$ at all boundaries [45]. For TE-polarized illumination, the boundary conditions at any planar boundary $z = z_{\mathrm{B}}$ are

$$\begin{cases} E^-(x,z_{\mathrm{B}}) = E^+(x,z_{\mathrm{B}}) \\ \left.\dfrac{\partial E^-(x,z)}{\partial z}\right|_{z\,=\,z_{\mathrm{B}}} = \left.\dfrac{\partial E^+(x,z)}{\partial z}\right|_{z\,=\,z_{\mathrm{B}}} \end{cases}, \qquad (15)$$

where the superscripts $-$ and $+$ refer to the limits when approaching the boundary from the negative and the positive z direction, respectively. The boundary conditions for TM polarization are correspondingly

$$\begin{cases} H^-(x,z_{\mathrm{B}}) = H^+(x,z_{\mathrm{B}}) \\ \dfrac{1}{\epsilon^-(x,z_{\mathrm{B}})}\left.\dfrac{\partial H^-(x,z)}{\partial z}\right|_{z\,=\,z_{\mathrm{B}}} = \dfrac{1}{\epsilon^+(x,z_{\mathrm{B}})}\left.\dfrac{\partial H^+(x,z)}{\partial z}\right|_{z\,=\,z_{\mathrm{B}}} \end{cases}. \qquad (16)$$

2.2 BKK method

The BKK method for solving the wave equation inside the grating is based on the method presented by Burckhardt for analyzing phase gratings with sinusoidal dielectric constant [46]. Kaspar generalized the method for arbitrary periodic refractive index distributions and gratings with absorption losses [47]. Knop used the method for the analysis of transmission phase gratings with rectangular grooves [48], which can easily be generalized for the multilevel gratings treated here.

We consider gratings that consist of N slabs parallel to the xy plane, in each of which the refractive index is constant in the z direction (Fig. 3). In the x direction, each slab is assumed to consist of discrete regions of constant refractive index. The

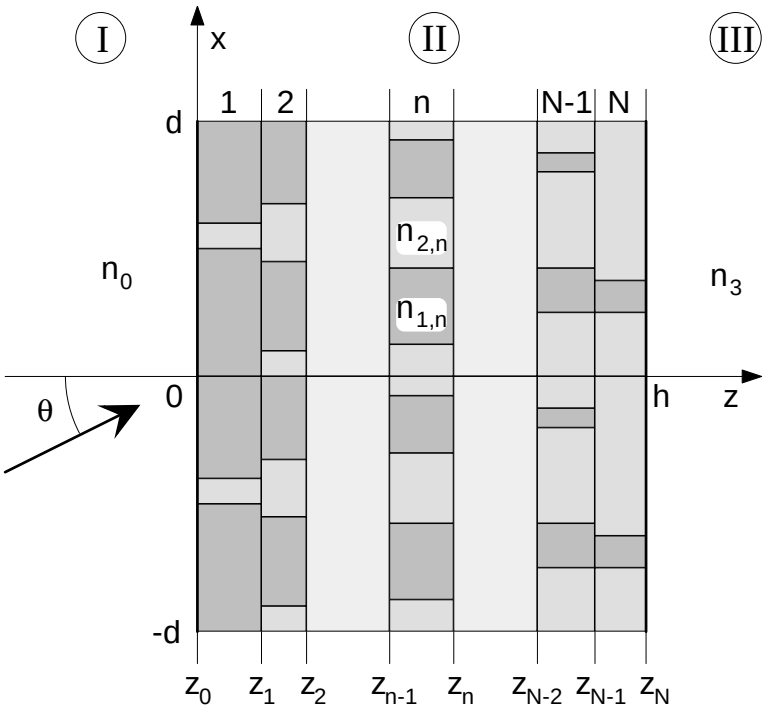

Figure 3: Diffraction of a plane wave by a multilevel lamellar grating: geometry of the modulated region.

special case of surface-relief gratings is obtained by defining a binary refractive index distribution $n_{1,\,n} = n_0$ and $n_{2,\,n} = n_3$. Equation (13) or (14) can be solved individually in each slab, and application of the boundary conditions (15) or (16) at the slab boundaries $z = z_n$ ($n = 0, \ldots, N$; $z_0 = 0$, $z_N = h$) gives the solution of the diffraction problem.

We search for a separable solution $U_{\mathrm{II},\,n}(x, z) = X_n(x)\, Z_n(z)$ for the field in the n:th slab ($z_{n-1} < z < z_n$) of region II. Presenting $[\epsilon_n(x)]^{-1}$ as a Fourier series expansion

$$\frac{1}{\epsilon_n(x)} = \sum_{q=-\infty}^{\infty} \zeta_{qn} \exp(i2\pi qx/d) \tag{17}$$

and denoting by γ_n the separation constant, Eqs. (13) and (14) are transformed into

$$\frac{\mathrm{d}^2 X_n(x)}{\mathrm{d}x^2} + \left[k^2 \sum_{p=-\infty}^{\infty} \varepsilon_{pn} \exp(i2\pi px/d) - \gamma_n^2 \right] X_n(x) = 0 \tag{18}$$

for TE polarization,

$$\sum_{p=-\infty}^{\infty} \varepsilon_{pn} \exp(i2\pi px/d) \frac{\mathrm{d}}{\mathrm{d}x} \left[\sum_{q=-\infty}^{\infty} \zeta_{qn} \exp(i2\pi qx/d) \frac{\mathrm{d}X_n(x)}{\mathrm{d}x} \right]$$

$$+\left[k^2\sum_{p=-\infty}^{\infty}\varepsilon_{pn}\exp(i2\pi px/d)-\gamma_n^2\right]X_n(x)=0 \tag{19}$$

for TM polarization, and

$$\frac{\mathrm{d}^2Z_n(z)}{\mathrm{d}z^2}+\gamma_n^2Z_n(z)=0 \tag{20}$$

for both states of polarization. These equations give the general solution

$$\begin{aligned}U_{\mathrm{II},n}(x,z) &= \sum_{j=1}^{\infty}\{A_{jn}\exp[i\gamma_{jn}(z-z_{n-1})]+B_{jn}\exp[-i\gamma_{jn}(z-z_n)]\}\\ &\quad\times\sum_{m=-\infty}^{\infty}F_{mjn}\exp(i\alpha_m x)\end{aligned} \tag{21}$$

The coefficients γ_{jn} and F_{mjn} are obtained from the eigenvalue equation

$$\sum_{m=-\infty}^{\infty}D_{pmn}F_{mn}=\gamma_n^2F_{pn}\ ,\ p=-\infty,\ldots,\infty, \tag{22}$$

where for TE polarization

$$D_{pmn}=k^2\varepsilon_{p-m,n}-\alpha_m^2\delta_{pm} \tag{23}$$

and for TM polarization

$$D_{pmn}=k^2\varepsilon_{p-m,n}-\sum_{q=-\infty}^{\infty}\varepsilon_{p-q,n}\zeta_{q-m,n}\alpha_q\alpha_m. \tag{24}$$

The continuity relations yield a doubly-infinite linear equation system at each of the $N+1$ boundaries. The unknown coefficients A_{jn} and B_{jn} as well as R_m and T_m may be solved from these equations. If the permittivity is constant in the z direction throughout region II, or $N=1$, the linear equation system can be simplified and its dimension reduced by one half by first eliminating R_m and T_m.

In the numerical implementation of the BKK method, the infinite series are truncated by retaining only L Rayleigh orders in an interval $[L_1,L_2]$ with $L=L_2-L_1+1$. An $L\times L$ dimensional eigenvalue problem arises for each slab. Accordingly, for each boundary, a linear equation system comprising $2L$ equations is obtained, so the total dimensions of the boundary condition matrix are $2L(N+1)\times 2L(N+1)$. However, the matrix is sparse, because a coupling between A_{jn} and B_{jn} exists only between successive slabs. The solution of the linear equation system can thus be implemented efficiently using Gauss elimination by storing in the computer memory only a small fraction of the coefficient matrix at a time [49, 50].

The BKK algorithm is currently implemented in XL FORTRAN programming language on IBM RS/6000 workstations running AIX 3.2.4 operating system. The eigenvalue equation and the linear equation system are solved using the ESSL subroutine library [51]. The memory capacity allows the inclusion of a maximum of approximately 900 Rayleigh orders for binary gratings, while for multilevel gratings the maximum is 450. The computation time is proportional to L^3; one evaluation of a two-level grating using 801 Rayleigh orders consumes 17 CPUmin for TE polarization and 22 CPUmin for TM polarization.

The number of Rayleigh orders that must be included to guarantee satisfactorily stabilized results depends primarily on the structure and the material of the grating, i.e., the variations in the refractive index. As a rule of thumb, assuming a customary index modulation of 0.5, all transmitted propagating orders and a number of evanescent orders must be included. The higher the steps in the refractive index distribution, and the more imaginary the refractive indices for metallic materials, the more additional evanescent orders are needed. Furthermore, the convergence of the results as the number of Rayleigh orders is increased is significantly slower for TM mode than for TE mode. This difference is crucial especially for highly conducting metallic gratings.

2.3 PCM method

A perfect conductor is an idealization for a highly conducting metal, in which the resistance inside the material is assumed to vanish. Consequently, the electric field must also vanish, and the boundary conditions at the interface between perfectly conducting and dielectric materials become particularly simple: the **E** vector on the dielectric side is perpendicular to the surface, whereas the **H** vector is parallel to the surface.

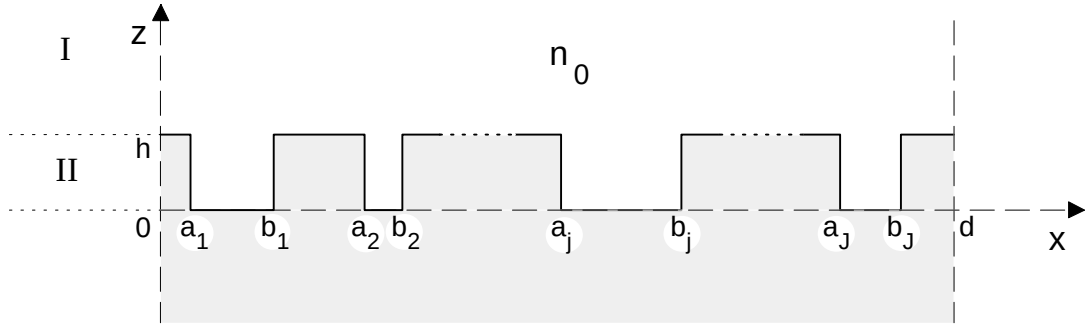

Figure 4: Geometry for a perfectly conducting lamellar grating.

We consider a perfectly conducting lamellar grating structure depicted in Fig. 4 containing J grooves with the boundaries a_j and b_j, and apply the waveguide-mode theory [8, 52, 53] extended to accept several grooves within one period [54, 55], which we call the perfect conductor modal (PCM) method. For the TE-polarized case, the field inside the j:th groove can be represented by a modal expansion

$$U_{\mathrm{II},\,j}(x,z) = \sum_{m=1}^{\infty} A_{mj} \sin(\mu_{mj} z) X_{mj}(x), \tag{25}$$

where $x \in (a_j, b_j)$, $\mu_{mj}^2 = (n_0 k)^2 - (m\pi/c_j)^2$, $c_j = b_j - a_j$, and

$$X_{mj}(x) = (2/c_j)^{1/2} \sin[m\pi(x - a_j)/c_j]. \tag{26}$$

A similar expression holds for TM polarization but with cosine terms substituted for the sine terms. The mode amplitudes A_{mj} and the Rayleigh coefficients R_n can be solved from the linear system obtained by matching the fields at $z = h$, by applying the method of moments, and by making use of the orthogonality relations of $X_{mj}(x)$ and the Rayleigh modes $\phi_n(x) = \exp(i\alpha_n x)/\sqrt{d}$.

2.4 Other methods

In addition to the BKK and the PCM method, a variety of rigorous algorithms have been presented [4,14,56]. We give here a brief review of the most widely used methods.

In the currently very popular coupled-wave method, the field inside the grating is expressed as a series of space-harmonic terms that correspond to the diffraction orders outside the grating. The orders are coupled and thereby exchange energy with each other. The rigorous coupled-wave (RCW) method was presented by Moharam and Gaylord for dielectric and metallic sinusoidal planar gratings [57, 58] and generalized to surface-relief gratings [49] and to the three-dimensional case of conical incidence [59]. The method has also been generalized to anisotropic gratings [60]. The RCW method is in principle rather similar to the BKK method and they are equivalent with respect to their results [61–63]. However, the RCW method is computationally more laborious, because the eigenvalue problem to be solved is twice the size compared with the BKK method.

The modal method is applicable to multilevel lamellar gratings with well-defined groove boundaries. Here, the field inside the grating is represented as an eigenmode expansion, in which each eigenmode analytically satisfies the wave equation and the

boundary conditions at the interfaces between the grooves. The modal method was first introduced for perfectly conducting lamellar gratings [52]. Botten and McPhedran generalized the method to dielectric and metallic lamellar gratings with a single groove in each period [64–66]. Botten's method can be generalized further to multiple grooves per period by applying the stratified medium matrix theory. The modal method is accurate and efficient even for highly conducting metallic gratings in TM polarization provided that the complex eigenvalue problem involved can be solved satisfactorily; however, finding all eigenvalues numerically is not straightforward, although the BKK method can be used to determine initial values for the search. In terms of speed of convergence, the modal method outperforms clearly both the BKK and the RCW method for metallic gratings in TM polarization [67].

Fourier methods such as the BKK and the RCW methods suffer from poor convergence caused, e.g., by Gibbs phenomenon at the boundaries. To eliminate this disadvantage, Morf has suggested an interesting approach where the field is represented as a superposition of Legendre polynomials separately in each region of constant refractive index [68]. The application of boundary conditions yields a conventional eigenvalue problem that is claimed to be free from the numerical problems of the modal method.

In the differential method, instead of determining the analytic series expressions for the field inside the grating as in the above-mentioned methods, the reflection and the transmission matrices that relate the reflected and the diffracted field to the incident field are determined by numerical integration through the grating. It is relatively easy to implement the method efficiently by utilizing classical integration algorithms such as Runge-Kutta and Numerov algorithms.

Integral methods differ significantly from the above-mentioned methods that are based on the solution of differential equations. In the method developed by Maystre [14, 69] the field is represented as an integral of an unknown function $\phi(x)$ over a given boundary that separates the two half-spaces. In the case of a perfectly conducting grating $\phi(x)$ corresponds to the surface current density, but it has no direct physical significance for dielectric or finitely conducting gratings. The field outside the surface-relief grating is obtained by solving $\phi(x)$ from the integral equations derived from the Helmholtz equation and the boundary conditions. The method can be generalized to gratings containing several layers of different materials. Integral methods are in general rather complicated theoretically and numerically, but they are very stable and perform well even for deep metallic gratings. One advantage of integral methods is that continuous boundaries can be handled accurately, whereas in the above-mentioned methods the boundaries must be discretized into slabs, thereby be-

ing approximated by staircase-like structures. On the other hand, integral methods are not suitable for graded-index gratings such as sinusoidal holographic volume gratings. Their applicability to discontinuous profiles such as binary gratings is questionable as well; the profile may be approximated by its truncated Fourier-series representation, but the convergence is not always satisfactory due to Gibbs phenomenon.

In this work we use mainly the BKK method because of its versatility and efficiency in the numerical implementation, although it can not compete, e.g., with the modal method for metallic gratings in TM polarization.

3 Fourier-type diffractive elements

Fourier-type diffractive optical elements generate the desired diffraction pattern in the far field. The spatial frequency spectrum of a Fourier-domain element can be observed at a finite distance by using a Fourier transforming lens [1].

3.1 Design concepts

The goal of the design process is to find grating structures that generate diffraction orders with a specified intensity distribution within the signal window $\mathcal{W}$. We consider here binary signals described by a goal power spectrum

$$\mathcal{P} = \{\hat{\eta}_m \mid \hat{\eta}_m \in \{0, 1\}, m \in \mathcal{W}\}. \tag{27}$$

The number of signal orders within the signal window with equal nonzero efficiencies is

$$N_s = \sum_{m \in \mathcal{W}} \hat{\eta}_m. \tag{28}$$

To characterize the fidelity of the element, we define the diffraction efficiency inside $\mathcal{W}$ as

$$\eta = \sum_{m \in \mathcal{W}} \hat{\eta}_m \eta_m, \tag{29}$$

where the efficiencies η_m are defined by Eq. (11) or (12), and the reconstruction error or the uniformity error

$$E = \max_{m \in \mathcal{W}} \left\{ \hat{\eta}_m \left| 1 - \frac{N_s \eta_m}{\eta} \right| \right\}, \tag{30}$$

which describes the maximum relative deviation from $\mathcal{P}$. Sophisticated paraxial-domain optimization algorithms may then be employed to find solutions with maximal η and minimal E [55, 70–73].

3.2 Fourier-domain designs

Fourier optics

In Fourier optics [1] all polarization, multiple-scattering, and volume effects inside the grating structure and usually also the reflections at the boundaries are ignored. The

influence of the refractive index modulation $n(x,z)$ is thus described by the phase delay of the wave propagating through region II, the so-called phase function, which for normal incidence takes the form

$$\phi(x) = k \int_0^h n(x,z)\mathrm{d}z. \tag{31}$$

The transmitted field is then obtained by multiplying the incident field by the transmission function

$$t(x) = \exp[i\phi(x)], \tag{32}$$

which shares the periodicity of $n(x,z)$. The complex amplitudes of the transmitted diffraction orders are the Fourier coefficients of $t(x)$ given by

$$T_m = \frac{1}{d} \int_0^d t(x) \exp(-i2\pi mx/d)\mathrm{d}x. \tag{33}$$

In the paraxial approximation, neglecting the Fresnel reflections, the efficiencies (12) of the diffraction orders reduce to $\eta_m = |T_m|^2$ for both states of polarization.

Binary phase gratings

A common grating geometry is the binary lamellar profile illustrated in Fig. 5 (cf. Fig. 4). Binary phase gratings can be used to split the incident wave into an array of beams with equal intensities; such elements are usually called Dammann gratings [74]. They are especially attractive due to the numerous applications of array illumination and multiple imaging in digital micro-optics and optical information processing [75–77]. Defining the J grooves of the lamellar profile by a set of transitions points $\{a_j, b_j\}$, the transmission function of a Dammann grating can be written as

$$t(x) = \begin{cases} 1, & \text{when } a_j < x < b_j \\ \exp(i\Delta\varphi), & \text{when } b_j < x < a_{j+1} \end{cases} \tag{34}$$

with $a_{J+1} = a_1 + d$ and the phase delay $\Delta\varphi = kh(n_3 - n_0)$. A customary choice is $\Delta\varphi = \pi$. From a fabrication point of view, the critical quantity is the minimum feature size

$$\Delta_{\min} = \min_{j=1,\ldots,J} \{b_j - a_j, a_{j+1} - b_j\}, \tag{35}$$

which should be maximized in the optimization.

An important type of Dammann grating is the so-called EOM (even orders missing) grating. These designs satisfy the condition $\phi(x+d/2) = \phi(x)+\pi$, i.e., the transitions

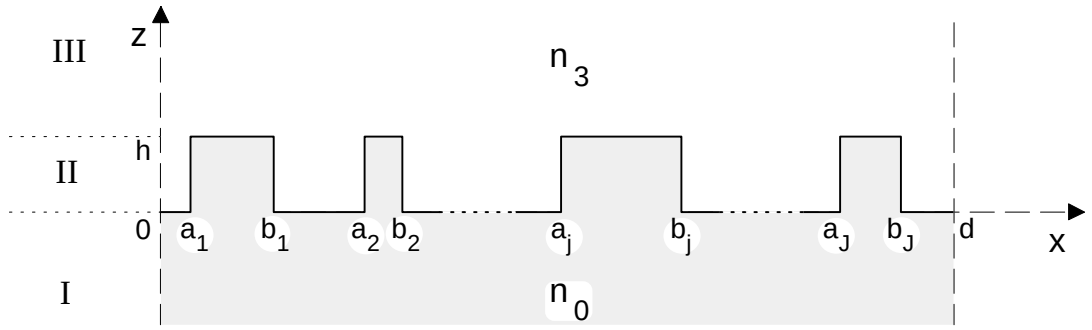

Figure 5: Geometry for a transmission-type binary phase grating.

of the first half of the grating period are replicated in the second half, but the phase values are reversed, which implies that no power is diffracted to the even diffraction orders. An advantage of EOM gratings is their lower sensitivity to fabrication errors: the zeroth order, which is most easily affected, does not contribute to array uniformity.

To investigate the validity of the Fourier-optics designs, the BKK method was used to analyze the performance of ordinary Dammann grating solutions that produce arrays of 7, 15, and 33 beams, as well as EOM-type designs with fan-out of 8, 16, and 32 [36]. The Fourier-optical characteristics of these gratings are given in Table 1. We assume normal incidence from glass ($n_0 = 1.5$) to air ($n_3 = 1$) and the groove depth $h = \lambda$. Normalized diffraction efficiencies η/η_F, where η_F is the Fourier-optical paraxial efficiency corrected by the Fresnel reflection, and uniformity errors are plotted in Fig. 6 as a function of grating period for TE-polarized illumination. To take into account the angular spread of the signal window $\mathcal{W}$ described by Eq. (10), the period values are divided by the highest diffraction order within $\mathcal{W}$, $N_{\max} = (N_s - 1)/2$ for ordinary designs and $N_{\max} = N_s - 1$ for EOM designs. This kind of approach can be used to analyze the general validity of the paraxial approximation in diffractive optics [24].

These curves demonstrate clearly the failure of Fourier-optics designs in the so-called resonance domain, in which the characteristic feature sizes are comparable to the wavelength of light. For ordinary Dammann gratings, the uniformity error increases substantially as period is reduced below $\sim 20 N_s \lambda$, although no distinct transition point can be defined because of the smoothness of the curves. For EOM designs, on the other hand, there is an abrupt deterioration of uniformity and a reduction of diffraction efficiency (due to power loss into even orders) at $d \sim 4 N_s \lambda$. Above this limit the performance figures converge rapidly to the values predicted by Fourier optics. This suggests that EOM gratings are considerably less sensitive than ordinary Dammann

N_s	η_F	E_F	$\Delta_{\min}/d$	J
7	0.7867	0.0043	0.1008	2
15	0.8177	0.0071	0.0625	4
33	0.8081	0.0120	0.0222	9
8	0.7152	0.0086	0.0500	5
16	0.8007	0.0065	0.0222	9
32	0.8183	0.0026	0.0118	17

Table 1: Fourier-optical characteristics of several ordinary and EOM-type Dammann gratings.

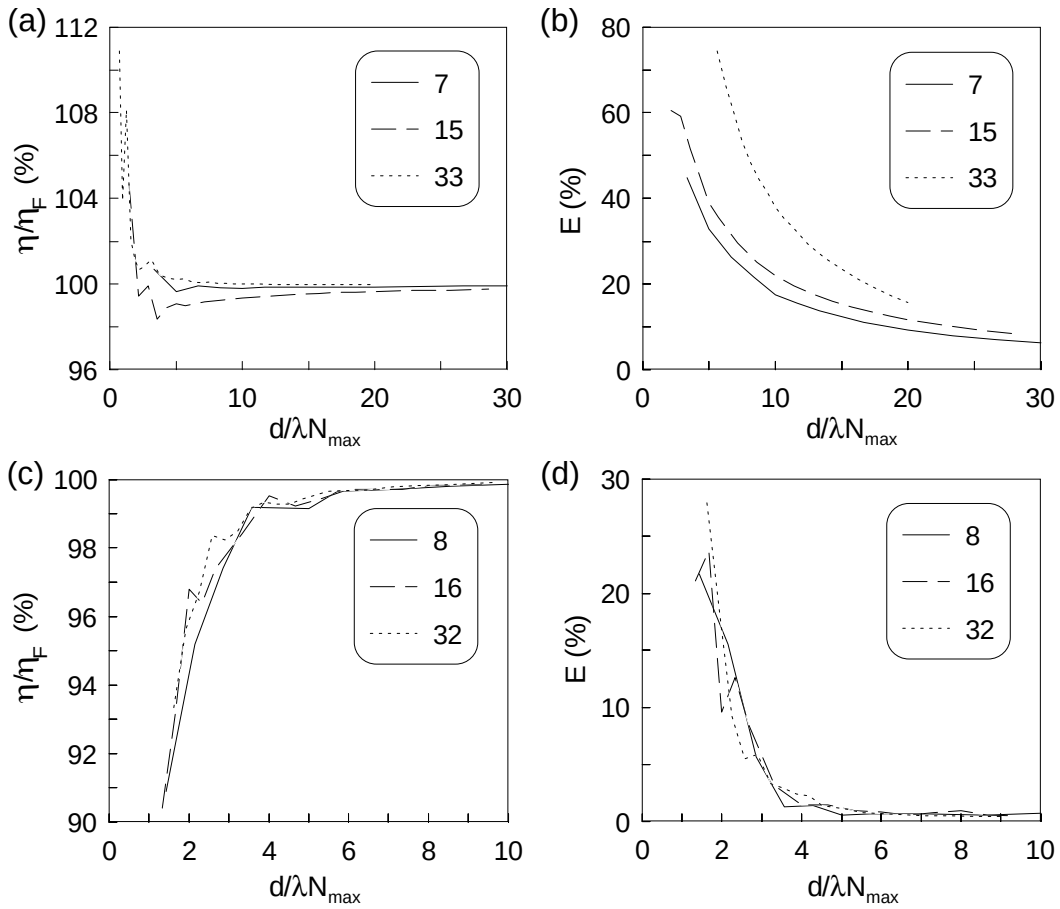

Figure 6: (a) Normalized efficiencies and (b) uniformity errors for Dammann gratings with fan-out to 7, 15, and 33 as a function of the normalized period $d/\lambda N_{\max}$, assuming TE-polarized illumination. Figures (c) and (d) are the same for EOM-type designs with fan-out to 8, 16, and 32. (Adapted from Ref. 36.)

gratings to resonance and scattering effects.

Multilevel phase gratings

Multilevel phase gratings (sometimes called kinoforms [78]) can be used instead of binary profiles, e.g., for high-efficiency array illumination. The number of levels in the surface-relief profile is typically a power of 2, which is suitable for VLSI-based fabrication processes. The transition points can be chosen quite freely and written with an accuracy of 0.5 μm [37].

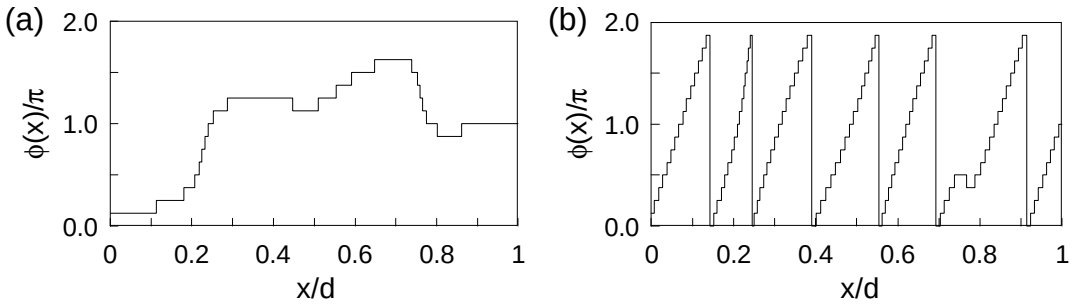

Figure 7: Phase relief profiles for (a) on-axis and (b) off-axis (Q = 6) array illuminators with fan-out to 6.

We consider several on-axis and off-axis array-illuminator solutions with even fan-out into the signal windows $\mathcal{W} = \{-N_s/2 + 1, ..., N_s/2\}$ and $\mathcal{W} = \{N_s/2 + 1, ..., 3N_s/2\}$, respectively. The phase relief profiles of such designs always contain one phase jump of π radians. As an example, the profiles of the on-axis and the off-axis designs for fan-out to 6 are shown in Fig. 7. For off-axis designs, the reconstructed array is shifted by Q orders by introducing an additional linear phase term $\phi_s(x) = 2\pi Q x$, which results in a sawtooth-like structure with Q phase jumps of 2π radians. This diminishes considerably the effect of the fabrication errors in the phase levels [79, 80]; on the other hand, the patterning accuracy of the transition points becomes more critical.

The BKK method is used to analyze the transition from the Fourier domain to the resonance domain. The results for several on-axis and off-axis grating solutions are shown in Fig. 8 similarly to the case of Dammann gratings in Fig. 6. The Fourier-optical diffraction efficiencies of the elements with fan-out to 4, 6, 8, and 16 are 90.6%, 88.0%, 94.5%, and 95.7%, respectively.

The reconstruction errors approach the Fourier-optics values ($E \lesssim 1\%$) more slowly than in the case of EOM-type Dammann gratings with equal fan-out. The diffraction

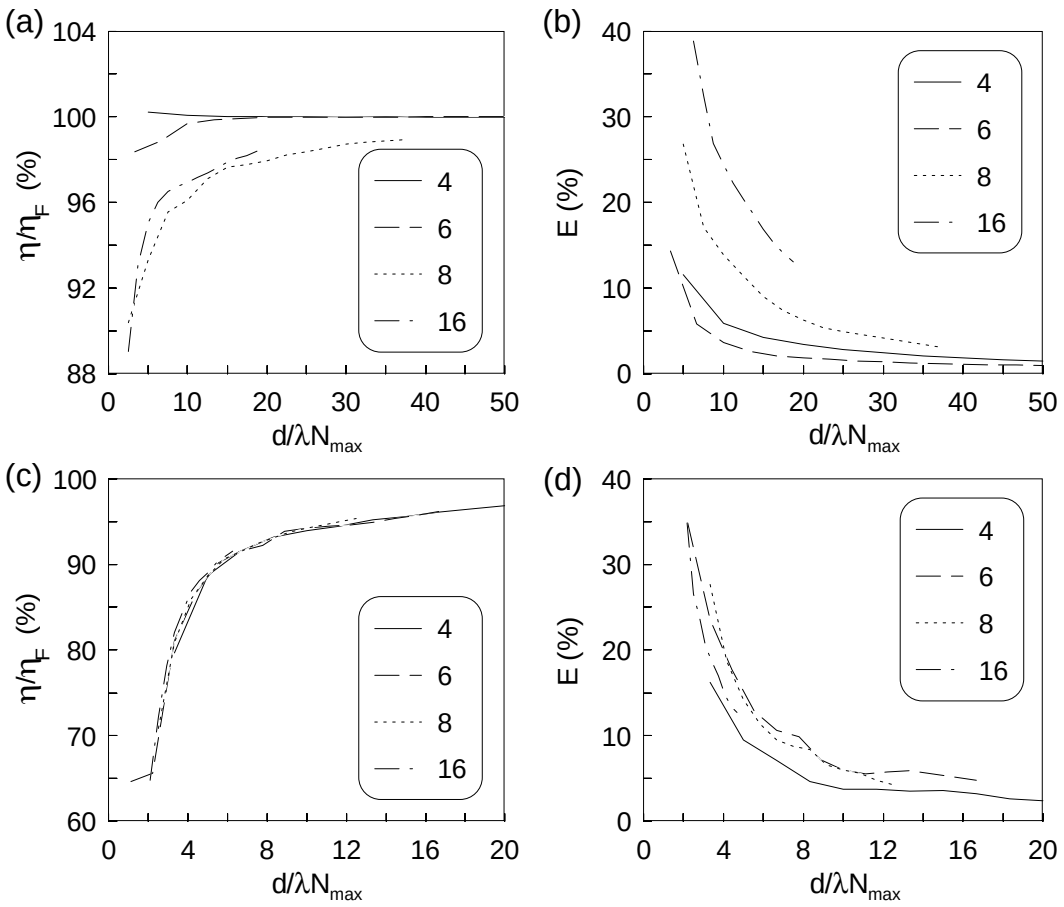

Figure 8: (a) Normalized efficiencies and (b) uniformity errors for on-axis multilevel array illuminators with fan-out to 4, 6, 8, and 16 as a function of the normalized period d/N_{max}, assuming TE-polarized illumination. Figures (c) and (d) are the same for off-axis designs. (Adapted from Ref. 37.)

efficiencies of the on-axis designs with a low fan-out to 4 and 6 stabilize quickly at the Fourier-optical predictions (corrected by the Fresnel reflection) when the grating period is increased. This is related to their rather smooth phase relief profiles [Fig. 7(a)] that do not contain phase jumps of 2π radians. For larger fan-out the convergence is gradual. In particular, the slow convergence of the results for the off-axis designs can be understood by interpreting them as phase-modulated sawtooth gratings with Q teeth per period [Fig. 7(b)]: the performance improves only after the average distance between the teeth exceeds about 10λ (Paper III).

3.3 2-D resonance-domain elements

As shown in Section 3.2, Fourier-optics designs begin to fail when the grating period d is reduced and the characteristic feature sizes of the grating structure become comparable to the wavelength of light. Since the volume and polarization effects ignored by Fourier optics are dominating in the resonance domain, the analysis and the design of such gratings must be based on electromagnetic diffraction theory [4].

Resonance domain synthesis of diffractive optical elements involves several fundamental differences compared with Fourier domain. In the resonance domain, the diffraction is highly dependent on the state of polarization and the angle of incidence of the illuminating wave. Evanescent waves also contribute significantly to the field inside the grating and can not be neglected. Furthermore, rigorous theory lacks the various symmetries present in Fourier optics, e.g., the general inversion symmetry of the diffraction pattern for binary gratings. Such a symmetry exists rigorously only if the grating profile itself is symmetric. The new degrees of freedom offered by these properties allow us to design elements with enhanced performance compared with their conventional counterparts (Ref. [55], Paper I). On the other hand, it is possible to synthesize new types of components, e.g., whose operation is controlled by the state of polarization.

We aim to control the diffracted field in a full half-space; i.e., we restrict the period length to such a range that the signal window contains all the reflected or the transmitted propagating orders: $\mathcal{W} = \mathcal{R}$ or $\mathcal{W} = \mathcal{T}$. This implies that no power is lost into unwanted diffraction orders and high diffraction efficiencies can be obtained. A perfect efficiency of $\eta = 1$ is always attained in the case of perfectly conducting reflection gratings, whereas the unavoidable reflections reduce somewhat the diffraction efficiencies of dielectric transmission gratings.

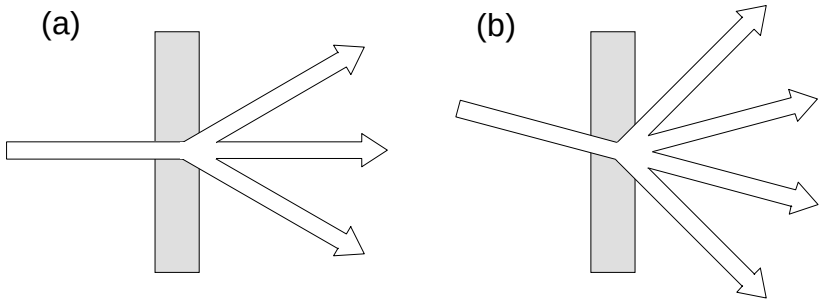

Figure 9: Geometry for (a) odd fan-out at normal incidence and (b) even fan-out at Bragg incidence for a transmission grating.

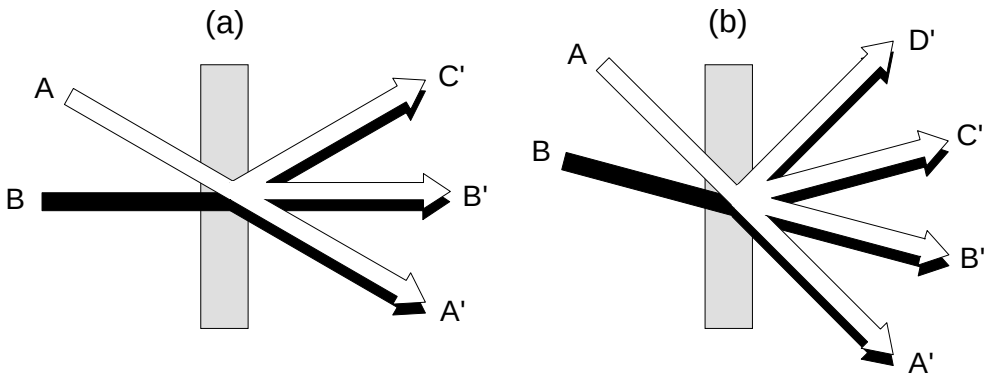

Figure 10: The operation of a star coupler connecting N sources to N detectors: (a) odd fan-out, (b) even fan-out at Bragg incidence. (The omitted inputs are mirror images of the illustrated inputs.)

The number of signal orders N_s (fan-out) is always odd for normal incidence, as illustrated for a transmission grating in Fig. 9(a). However, an even fan-out can be achieved by setting the incident wave at the Bragg angle θ_B with $\sin\theta_B = \lambda/(2n_0 d)$, as shown in Fig. 9(b).

Optimization results for several dielectric and perfectly conducting fan-out gratings are summarized in Table 2 assuming TE polarization. Lamellar geometry is used with $n_0 = 1.5$ and $n_3 = 1$ for the dielectric solutions and with $n_0 = 1.0$ for the perfectly conducting reflection gratings. Because of the strong polarization dependency, these designs fail completely when illuminated by TM-polarized light. However, the optimization can be carried out similarly for TM polarization or as well simultaneously for both states of polarization if polarization-insensitive operation is desired.

As an example of the synthesis involving several input waves we consider the so-called star coupler [81]. It is a diffractive element that connects each of the N mutually uncorrelated sources A, B, C, etc. to all of the N receivers A', B', C', etc. (Fig. 10). Table 3 gives the solutions for dielectric and perfectly conducting 3-to-3 and 4-to-4 star couplers. A symmetric lamellar profile is used here for both odd-numbered and even-numbered fan-out. This simplifies the optimization with the implication that the diffraction patterns at the angles of incidence θ and $-\theta$ are rigorously mirror images and thereby equivalent for our purpose.

The high polarization sensitivity of the diffraction in the resonance domain enables us to design gratings that generate different diffraction patterns at different states of polarization. A simple polarization-sensitive component is the polarization beam splitter, which passes light straight through in one state of polarization and diffracts the other

N_s	η (%)	E (%)	d/λ	h/λ	$\theta(^\circ)$	$\Delta_{\min}/\lambda$	J
2	97.2	0.6	1.00	0.76	19.48	0.45	1
3	95.1	3.2	1.83	0.93	0.00	0.28	1
4	94.3	1.6	2.16	0.93	8.88	0.26	2
5	93.8	1.2	2.73	0.82	0.00	0.48	2
6	94.5	3.0	3.16	0.85	6.06	0.46	2
7	94.5	3.0	3.86	0.83	0.00	0.59	2
8	90.1	2.5	4.19	1.04	4.56	0.50	3
9	93.3	3.0	4.86	1.26	0.00	0.46	3
2		0.7	1.48	0.23	19.75	0.66	1
3		2.7	1.97	0.19	0.00	0.91	1
4		4.4	2.47	0.25	11.68	0.35	2
5		3.3	2.99	0.25	0.00	0.55	2
6		2.3	3.48	0.25	8.26	0.60	2
7		6.1	3.97	0.24	0.00	0.69	2
8		3.5	4.47	0.30	6.42	0.52	3
9		6.3	5.00	0.28	0.00	0.56	3

Table 2: Optimization results for dielectric (upper table) and perfectly conducting (lower table) fan-out gratings.

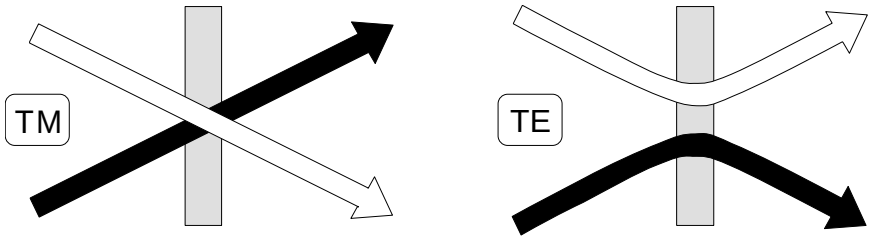

Figure 11: Operating principle of a polarization-sensitive node.

state of polarization into the first order. A polarization beam splitter can also be used as a polarization-sensitive node as illustrated in Fig. 11: two uncorrelated input beams incident at angles $\pm\theta$ are either passed through or swapped, depending on the state of polarization. By controlling the polarization state of the input beams, the component can be used like the conventional active nodes that are based, e.g., on acousto-optic or electro-optic Bragg diffraction.

It is also possible to achieve efficiencies in excess of the paraxial-domain upper bounds in the transitional domain [25]. For instance, the upper bound for a paraxial-domain beam splitter that generates two equal-efficiency orders ± 1 is $8/\pi^2 \approx 81\%$, but we have obtained efficiencies of $\sim$ 90% for periods as high as 7λ by using several small features instead of a single groove.

3.4 3-D resonance-domain elements

In Paper II we present an extension to the BKK method for doubly-periodic elements with three-dimensional surface relief profiles (also known as crossed gratings). Because of the numerical complexity of the method, accurate results can be obtained only for periods below 10λ if the refractive indices $n_0 = 1.5$ and $n_3 = 1.0$ are assumed. However, this is sufficient for the synthesis of diffractive optical elements to operate in the resonance domain. We consider binary profiles that consist of rectangu-

	Dielectric		Perfect conductor	
	3-to-3	4-to-4	3-to-3	4-to-4
$a_1/\lambda, b_1/\lambda$	0.104, 0.397	0.556, 0.676	0.000, 1.751	0.272, 0.554
$a_2/\lambda, b_2/\lambda$	1.376, 1.669	1.037, 1.457	–	0.608, 1.743
$a_3/\lambda, b_3/\lambda$	–	1.836, 1.956	–	1.797, 2.079
d/λ	1.773	2.512	1.946	2.351
h/λ	0.957	1.192	0.335	0.430
η_A	96.0%	88.9%	100%	100%
η_B	96.9%	88.2%	100%	100%
E_A	3.0%	1.3%	0.3%	0.9%
E_B	0.8%	1.0%	0.2%	0.9%

Table 3: Designs for dielectric and perfectly conducting 3-to-3 and 4-to-4 star couplers.

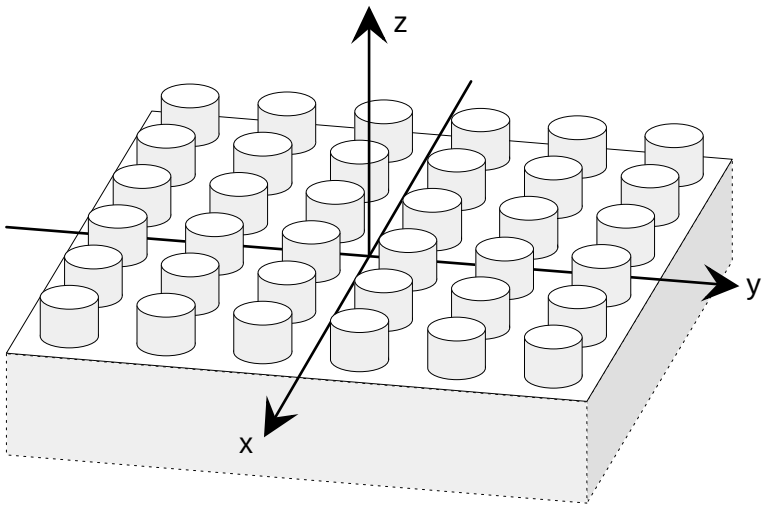

Figure 12: Geometry for a crossed grating with 3-D profile.

lar, circular, or trapezoidal features. At least circular subwavelength-domain features can also be realized with the use of modern microfabrication technology [82]; such a profile is illustrated in Fig. 12.

Symmetries similar to the 2-D case can be utilized to reduce the degrees of freedom and thus to simplify the optimization process. We have observed that a profile symmetric with respect to both coordinate axes and illuminated at normal incidence generates a diffraction pattern that is inversion symmetric irrespective of the state of polarization. In addition, if the polarization vector points along either coordinate axis, the spectrum possesses an axial mirror symmetry.

Some examples of 2-D beam-splitter designs with fan-out to 4, 6, and 9 are depicted in Fig. 13. The desired signal (solid circles denote the signal orders) and the top view of one grating period (shaded regions are occupied by the dielectric substrate) are shown for each element. The diffraction efficiencies of these designs are 80%, 93%, and 91%, respectively, with $\sim 10\%$ array uniformities. The fabrication tolerances for the elements of Figs. 13(a) and 13(c) are analyzed in Fig. 14, in which the uniformity errors are evaluated as a function of the deviations of the relief depth and the feature diameter (the optimal uniformities seem better than the actual values because of lower numerical accuracy). The $1 \rightarrow 9$ beam splitter is very sensitive in particular to errors in the feature size, whereas the uniformity of the $1 \rightarrow 4$ beam splitter is not as seriously affected, because the zeroth order is not a signal order and does not contribute to the uniformity.

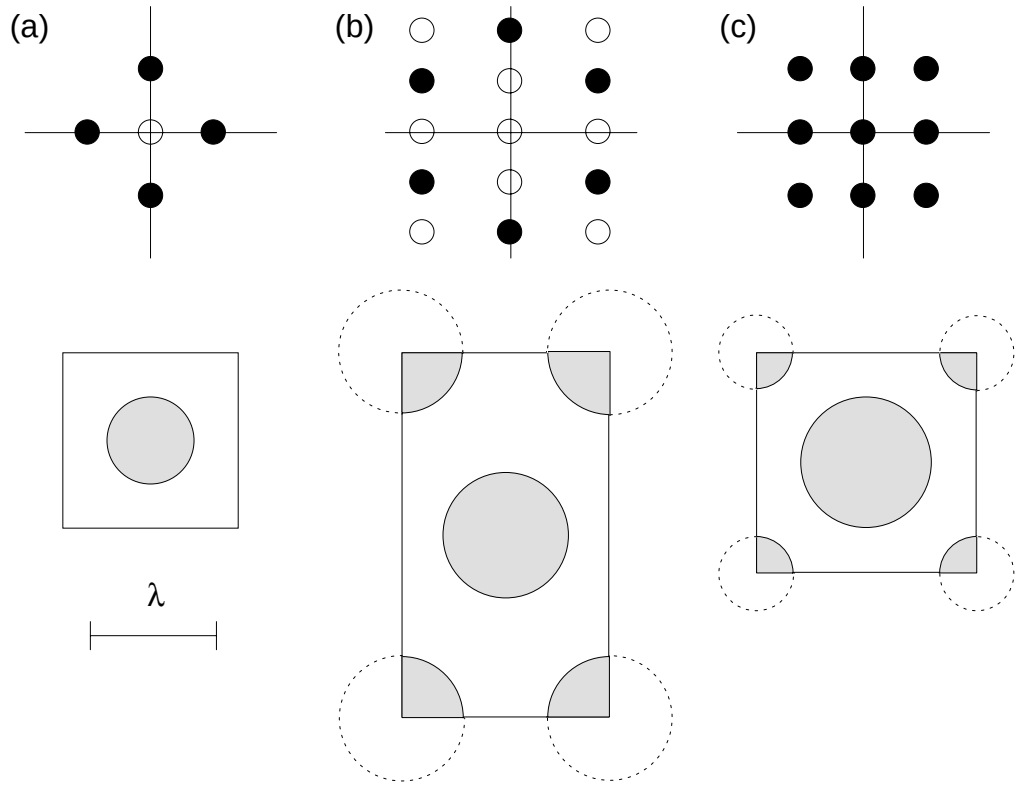

Figure 13: Examples of 2-D beam splitters: the desired signal and the top view of one grating period are shown for elements with fan-out to (a) 4, (b) 6, and (c) 9. The relief depths are (a) $h = 1.39\lambda$, (b) $h = 1.28\lambda$, and (c) $h = 1.57\lambda$.

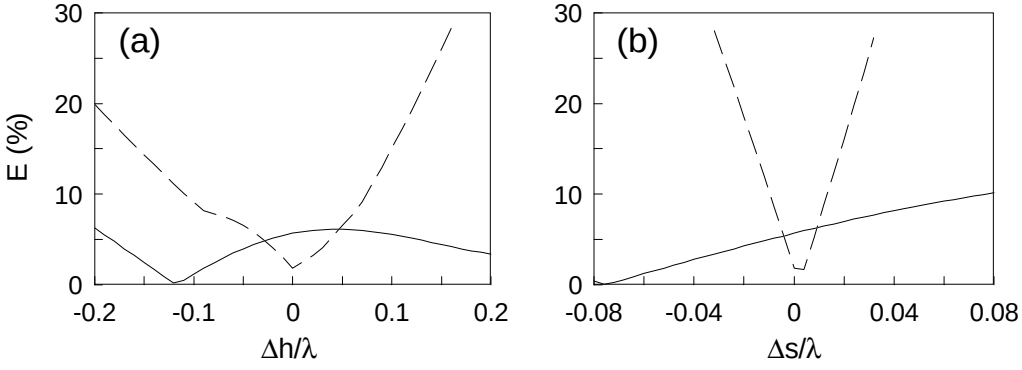

Figure 14: Effect of fabrication errors of (a) the relief depth h and (b) the feature size s on array uniformity error E evaluated for the $1 \rightarrow 4$ beam splitter of Fig. 13(a) (solid curves) and the $1 \rightarrow 9$ beam splitter of Fig. 13(c) (dashed curves).

4 Fresnel-type diffractive elements

In this chapter we consider diffractive optical elements that operate in the Fresnel domain; i.e., they generate the desired output in the Fresnel region of the aperture. Diffractive elements of this kind, such as micro Fresnel lenses and lens arrays [83], and multifacet holograms, are essentially synthetic interferograms, which can be treated locally as diffraction gratings. The variations of the local grating period across the aperture primarily determine the wave-front transformations produced by the element, whereas the local first-order efficiency depends on the grating groove shape. Therefore, to understand and to optimize the operation of a diffractive element, knowledge of the multilevel resonance-domain grating structures with staircase-like profiles is necessary.

4.1 Multilevel staircase gratings

Figure 15 illustrates the local grating structure of a diffractive element. For VLSI-based fabrication processes, the triangular surface-relief profile of Fig. 15(a) is quantized as shown in Fig. 15(b). The first-order efficiency of such staircase structures is investigated in Papers III and IV. The essential result is that the efficiencies remain clearly below the Fourier-optics predictions for grating periods $d < 10\lambda$ if the number of quantization levels is greater than two. In particular, whether the profile is quantized or not, there is a significant drop of efficiency at $d \approx 2\lambda$ for TE-polarized illumination incident from substrate to air (Fig. 16; see also Fig. 1 of Paper III). It is interesting to notice that such behavior can be predicted with a fair degree of accuracy for a prism-like structure by a simple approximate model based on the ideas of Beckmann [84]: light is assumed to propagate in the modulated region according to geometrical optics, and the Fresnel reflection and transmission coefficients are used at the boundaries (see Fig. 5 of Paper IV). The complex amplitude of the first diffraction order is then obtained as a Fourier coefficient of the transmitted field.

The drop of efficiency in the resonance domain can be eliminated through a rigorous optimization of the grating profile. For example, the optimized efficiency curves (with h either fixed or optimized) for a 4-level grating are compared with the nonoptimized efficiency curve in Fig. 16(a) (Fig. 6 of Paper IV slightly refined at the low end of the period range), whereas Fig. 16(b) shows the corresponding phases of the

first diffraction order. Optimization of the relief depth yields generally better efficiencies, but a fixed value of h is in practice required for the VLSI-based fabrication of elements with variable local period. Furthermore, phase variations cause aberrations in the operation of the diffractive element, but they can easily be eliminated by shifting the local grating structure according to the generalized [79] detour-phase principle of computer-generated holography [19].

The optimized grating profiles differ significantly from the nonoptimized profile depicted in Fig. 15(b), especially in the range $1.5 < d/\lambda < 4$ where the original efficiency is low. This is visualized in Fig. 17 for 4-level profiles with $d = 2\lambda$ and $d = 4\lambda$.

4.2 Diffractive-lens arrays

Microlens arrays may be interpreted as diffraction gratings that consist of adjacent micro Fresnel lenses [16, 83]. Their applications in optical computing and information processing include pickup lenses in compact disc players and coupler lenses in optical communication systems [83]. Microlens arrays can also be used in array generation [76, 85].

The ideal phase function of a lens that converts a normally incident plane wave into a converging cylindrical wave is

$$\phi(x) = k\left\{F - \left[F^2 + (x - d/2)^2\right]^{1/2}\right\} + \phi_0\,, \tag{36}$$

where F denotes the geometrical-optics focal length and $\phi_0 \in [0, 2\pi]$ is an arbitrary phase factor. This definition implies that the geometrical-optics focus is located at $(x, z) = (d/2, h + F)$. A blazed-type Fresnel lens is generated by modifying the ideal phase function to have a modulo 2π structure, which produces sawtooth-like Fresnel

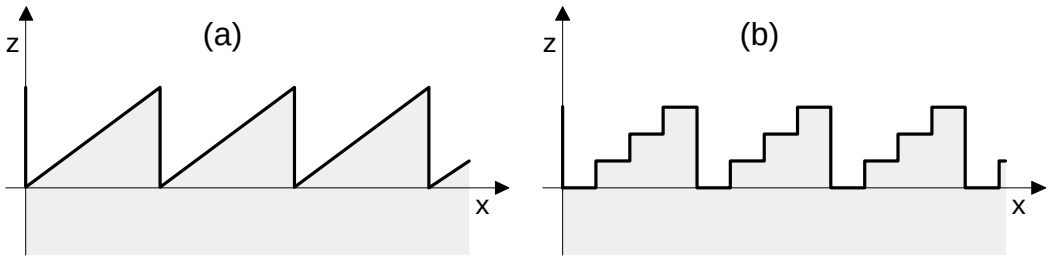

Figure 15: Geometry for sawtooth gratings. (a) Nonquantized profile, (b) quantized profile.

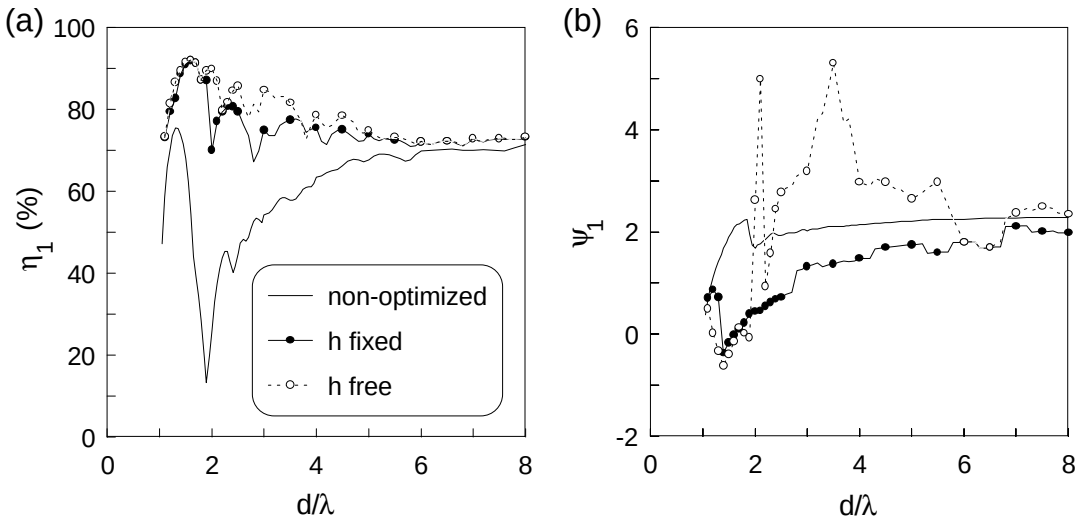

Figure 16: Results of the optimization of the local groove structure of a 4-level grating for TE polarization, compared with the nonoptimized case: (a) first-order efficiency η_1, (b) phase ψ_1 of the first diffraction order in radians.

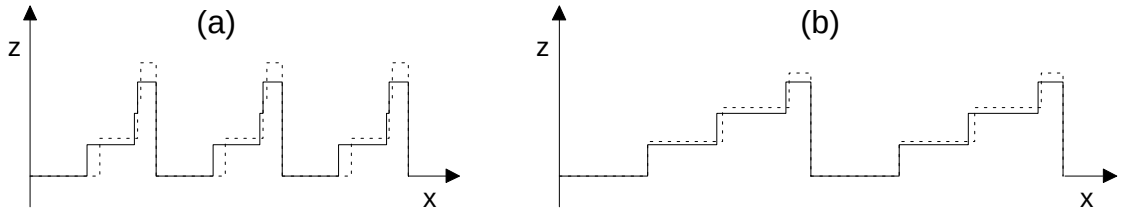

Figure 17: Optimized 4-level grating profiles at (a) $d = 2\lambda$ and (b) $d = 4\lambda$ with h fixed (solid curves) or h optimized (dotted curves).

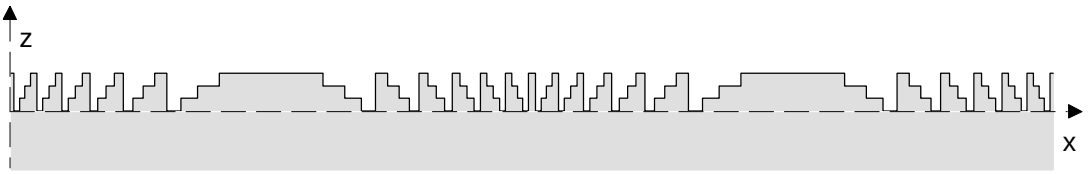

Figure 18: Nonoptimized profile of a lens array with a lens diameter of $d = 100\lambda$ and focal length $F = 200\lambda$ ($\phi_0 = 0$).

zones. Continuous phase distributions of this type can be fabricated as blazed surface-relief profiles with the use of, e.g., electron-beam [83] or laser-beam [86] lithography. For manufacturing by standard VLSI-based patterning [87], etching, or thin film deposition [88] techniques, the phase distribution is quantized to contain discrete phase levels in the range $[0, 2\pi]$.

In the conventional construction scheme, generalized Kirchhoff boundary conditions, which assume that the field propagates through the modulated region according to geometrical optics, are applied to obtain a surface-relief profile directly proportional to the phase profile [cf. Eq. (31)]. Such a profile is illustrated in Fig. 18. On the other hand, the lens profile may be constructed rigorously with the use of local period optimization and detour-phase aberration correction. Fig. 7 of Paper IV shows nonoptimized and rigorously optimized lens profiles with lens aperture $d = 100\lambda$ and focal length $F = 50\lambda$. The minimum local period is $d_L = 1.4\lambda$ at the edges of the aperture. The modifications are most pronounced in the range $20 < |x|/\lambda < 30$ (with $2 < d_L/\lambda < 2.5$) where the optimized profile essentially contains only three levels. The effect of optimization on the transmitted wave-front can be seen clearly in the phase $\phi(x)$ of the complex-amplitude transmission function plotted in Fig. 19 for the same lens array. Only the propagating orders are included in the calculation since the evanescent waves do not propagate to the focal plane. The distortions in the nonoptimized phase function are reduced significantly in the range $20 < |x|/\lambda < 30$, in good agreement with the local optimization results.

The enhancements produced by rigorous optimization can also be seen by evaluating the field intensity (defined as the z component of the time-averaged Poynting vector $\langle S_z \rangle$) around the focus. A remarkable increase of the peak intensity is observed in the focal-plane and the axial intensity profiles presented in Fig. 20. An approximate theory with Kirchhoff boundary conditions is used in the analysis for comparison with the electromagnetic theory; the diffracted field given by Fourier optics and corrected by the Fresnel transmission coefficient is propagated further rigorously by the Rayleigh

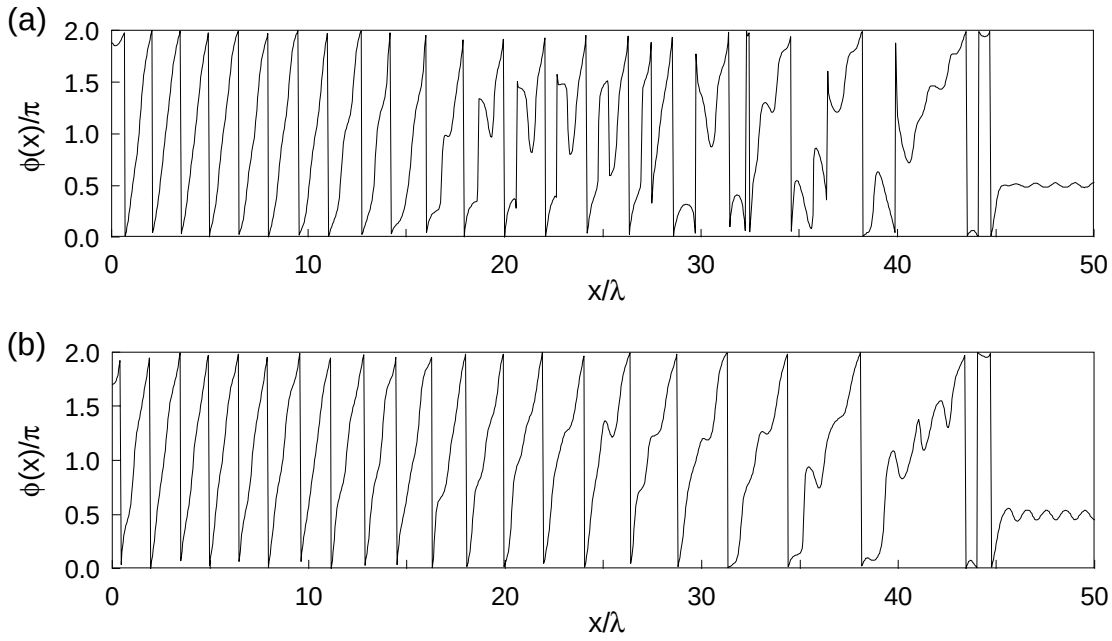

Figure 19: Phase of the complex-amplitude transmission function for an F:0.5 lens array with $d = 100\lambda$. (a) Construction using ideal phase function with Kirchhoff boundary conditions, (b) construction using rigorous optimization and detour-phase correction.

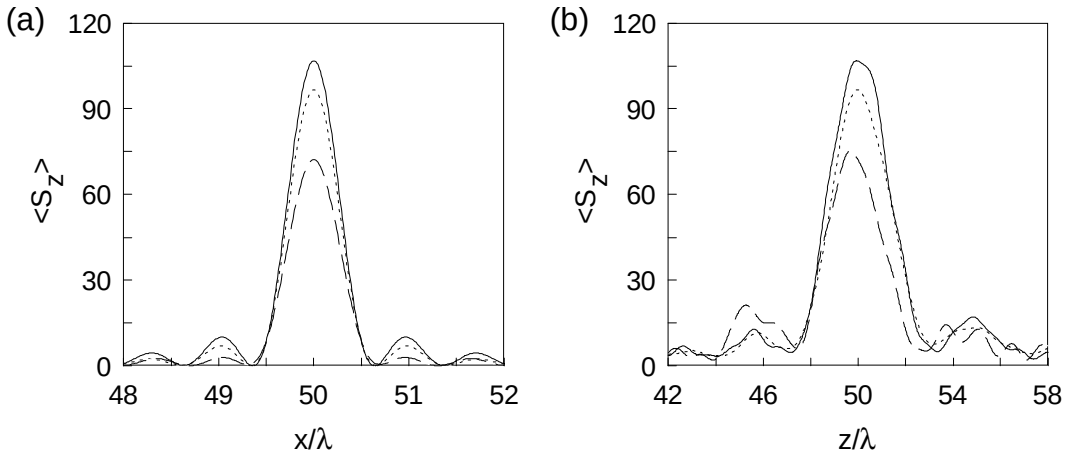

Figure 20: Intensity profiles (a) in the geometrical-optics focal plane $z = 50\lambda$ and (b) in the axial plane $x = 50\lambda$ for a F:0.5 lens array with $d = 100\lambda$. Solid lines, results for the rigorously optimized profile; dashed lines, results for the nonoptimized profile; dotted lines, prediction of the approximate theory.

expansion. On the other hand, we may also consider the influence of the optimization on the spatial power spectrum: the efficiencies of the transmitted diffraction orders are smoothed inside the Debye window [89], while the higher order efficiencies are reduced (see Fig. 9 of Paper IV).

4.3 Talbot effect

Periodic structures are known to form exact images of themselves at integer multiples of the distance $z_T = 2d^2/\lambda$ through Fresnel diffraction when illuminated by a coherent plane wave [15, 90–93]. This self-imaging phenomenon is called the Talbot effect. In addition, multiple phase-transformed Fresnel images are produced at the fractional-Talbot distances $z = (q + p/n)\, z_T$, where n, p, and q are integers [94,95]. For instance, n laterally shifted and equally spaced images with different phases are formed at the planes $z = z_T/(2n)$. A common element is the so-called Ronchi ruling that consists of alternating transparent and opaque bars of equal width. It generates a binary-amplitude image in the planes $z = (q + p/2)\, z_T$, whereas a uniform intensity distribution with binary-valued phase is produced in the planes $z = [q + (2p + 1)/4]\, z_T$. This kind of image formation may be reversed, i.e., amplitude-only images may be generated by gratings that consist of constant phase zones. The fractional Talbot effect has been applied to realize binary-phase [96, 97] and multilevel-phase [95] grating array illuminators that generate uniformly illuminated arrays of squares. The operation of such an array illuminator is comparable to that of micro-Fresnel lens arrays [83] discussed in Section 4.2.

In Paper V we consider lamellar grating structures depicted in Fig. 21 with one half of the period occupied by either a metallic material with refractive index $n_g = 3.48 + 4.36i$ (chromium at $\lambda = 620$ nm) or a dielectric material with $n_g = 1.5$. The grating is surrounded by dielectric ($n_0 = 1.5$) and air ($n_3 = 1$). The depth of the metal layer in the metallic Ronchi ruling is $h = 100$ nm, which causes practically total opaqueness for visible light. In the dielectric case, the phase delay of $\pi/2$ radians required in array generation by the fractional Talbot effect [96] is obtained with the relief depth $h = \lambda/2$. In both cases, the grating is illuminated by a TE-polarized wave at normal incidence.

The transmitted field in the exit plane of metallic and dielectric gratings is investigated in Figs. 2 and 3 of Paper V, respectively. As expected, the Kirchhoff boundary conditions are not satisfied and the field in the exit plane of the grating does not resem-

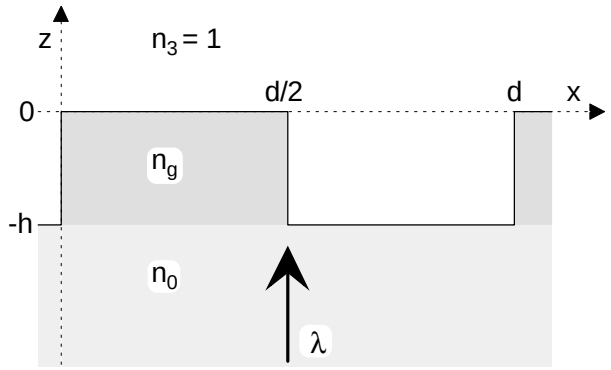

Figure 21: Grating geometry for the analysis of self-imaging.

ble the grating structure, whether or not the evanescent orders are included. Furthermore, the evanescent waves have considerable amplitudes and contribute significantly to the field in the exit plane but decay exponentially as the wave propagates in the z direction, so they can not be included in the self-imaging field. The concept of self-imaging in the rigorous sense is therefore inappropriate for physical objects such as gratings and is meaningful only for the propagating part of the diffracted field.

The intensity profiles for several metallic and dielectric gratings are evaluated (excluding the evanescent waves) in various Talbot and fractional-Talbot planes in Figs. 4–6 of Paper V. Some of the results for a metallic grating with $d = 9.9\lambda$ are reproduced in Fig. 22; the paraxial scalar theory now predicts binary-amplitude profiles in the planes $z = 0$, $z = z_T/2$, and $z = z_T$, whereas a binary-phase constant-intensity profile is expected in the quarter-Talbot plane $z = z_T/4$. The trend towards the predicted behavior can be seen especially for the binary-amplitude cases, although the exact shapes of the profiles do not justify the speaking of self-imaging. Heavy fluctuations are observed in the planes where a binary-phase constant-intensity profile is expected. The results of the Kirchhoff boundary conditions plotted with dotted lines are qualitatively similar to the rigorous results, but the quantitative differences are considerable particularly for the lower grating periods.

If only three diffraction orders propagate, which is the case for grating periods $1 < d/\lambda < 2$, the field is always self-imaging with distance

$$z_T = \frac{\lambda}{1 - \{1 - [\lambda/d]^2\}^{1/2}} \tag{37}$$

irrespective of the grating structure. Exact self-imaging of the homogeneous part of the transmitted field is possible also for five propagating orders if the grating period is chosen suitably in the range $2 < d/\lambda < 3$ (Paper V). Conditions for exact self-imaging

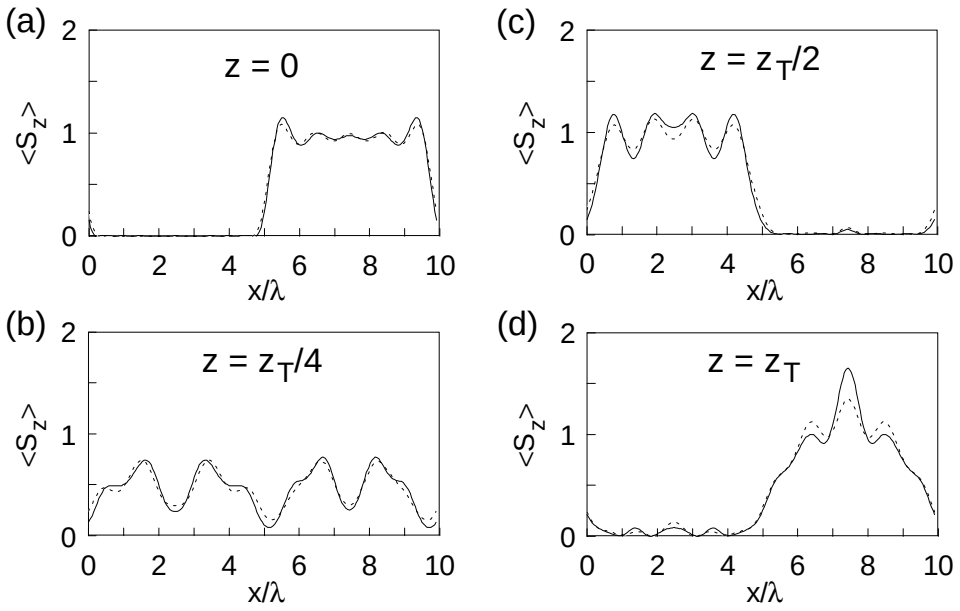

Figure 22: Lateral field profiles in several Talbot and fractional-Talbot planes for a metallic grating with $d = 9.9\lambda$. Solid lines, rigorous results; dotted lines, Kirchhoff results.

can be formulated as well for a larger number of propagating orders, but we have not been able to find any such solutions.

5 High-frequency-carrier elements

In this chapter we consider the method introduced in Ref. 98 for the synthesis of diffractive optical elements. Unlike the conventional methods to realize unconstrained phase functions through continuous-profile or multilevel elements, our method is based on pulse-frequency modulation of a binary high-frequency carrier grating. The optical function may be designed with the use of scalar theory, whereas the subwavelength structure of the carrier grating has to be optimized rigorously by electromagnetic theory.

5.1 High-frequency carrier gratings

We consider here binary rectangular-pulse gratings that should ideally diffract all incident power into the (minus) first diffraction order [99–102], as depicted in Fig. 23. The characteristic dimensions are the period d_c, the pulse width c, and the groove depth h. The illuminating wave is obliquely incident from a dielectric medium with refractive index n, typically at the Bragg angle $\theta_B = \arcsin[\lambda/(2nd_c)]$, in contrast to the multilevel staircase gratings studied in Section 4.1 that operate at normal incidence. Choosing the period in the range $0.5 < d_c/\lambda < 1.5$ and assuming Bragg incidence, only two diffraction orders (-1 and 0) propagate. The goal is to maximize the first-order efficiency η_{-1} by optimizing h (and possibly the aspect ratio c/d_c) for a chosen d_c. We are especially interested in solutions that are tolerant to fabrication errors or to deviations from the Bragg condition.

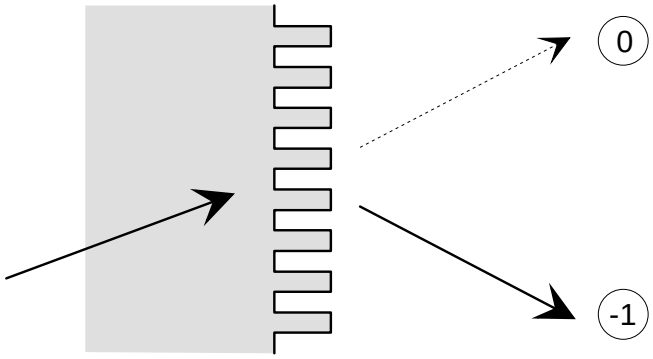

Figure 23: Geometry for a transmission-type binary high-frequency carrier grating.

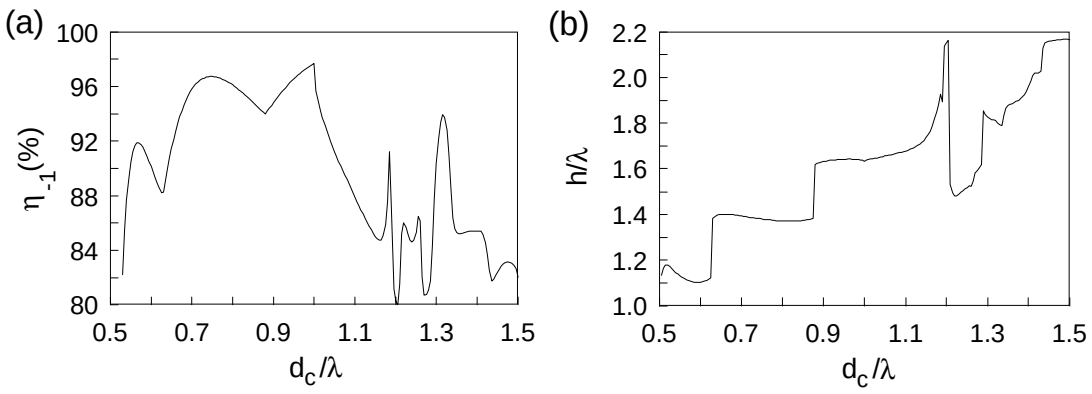

Figure 24: (a) Maximum first-order efficiency as a function of period d_c for a transmission-type binary high-frequency grating with $c/d_c = 0.5$ at Bragg incidence. (b) Optimal relief depth h for each d_c.

Figure 24 (reproduced from Fig. 3 of Paper VI) shows the optimized first-order efficiency η_{-1} and the corresponding relief depth h plotted as a function of d_c for a transmission-type grating with $c/d_c = 0.5$ in TE polarization. The five solutions with periods $d_c/\lambda =$ 0.6, 0.8, 1.0, 1.2, and 1.4 listed in Table 1 of Paper VI are analyzed further to evaluate the effects of errors in the angle of incidence, the aspect ratio, and the groove depth (Fig. 5 of Paper VI). The results indicate that a period of $d_c = \lambda$ is the most preferable; the first-order efficiency $\eta_{-1} = 97.7\%$ is then obtained with the groove depth $h = 1.635\lambda$. In general, the optimal value of the aspect ratio differs from 0.5: η_{-1} may be improved by as much as 10% if c/d_c is optimized.

For reflection-mode operation we use a grating geometry similar to Fig. 23 but assume a perfectly conducting substrate material and TM-polarized illumination. A first-order efficiency of 100% can now be achieved in the range $0.5 < d_c/\lambda < 1.18$ with $c/d_c = 0.5$, above which there is a sharp drop due to the nonoptimal aspect ratio. This range is favorable also in terms of tolerances to fabrication errors; a convenient choice is $d_c = \lambda$ with groove depth $h = 0.234\lambda$. Furthermore, for the lower periods $d_c < 1.2\lambda$, the Bragg-angle selectivity is considerably lower in reflection mode than in transmission mode, as shown in Fig. 8 of Paper VI. It is therefore possible to reach 100% efficiency at non-Bragg angles of incidence, where the diffracted beam is thus angularly separated from the illuminating beam. This is illustrated in Fig. 25, in which the relief depth is optimized for various grating periods as a function of the angle of incidence to give the maximum first-order efficiency η_{-1}. At a higher angle of incidence, however, there is an abrupt drop of efficiency at much smaller (positive) perturbations of the local period that are introduced through pulse-frequency modula-

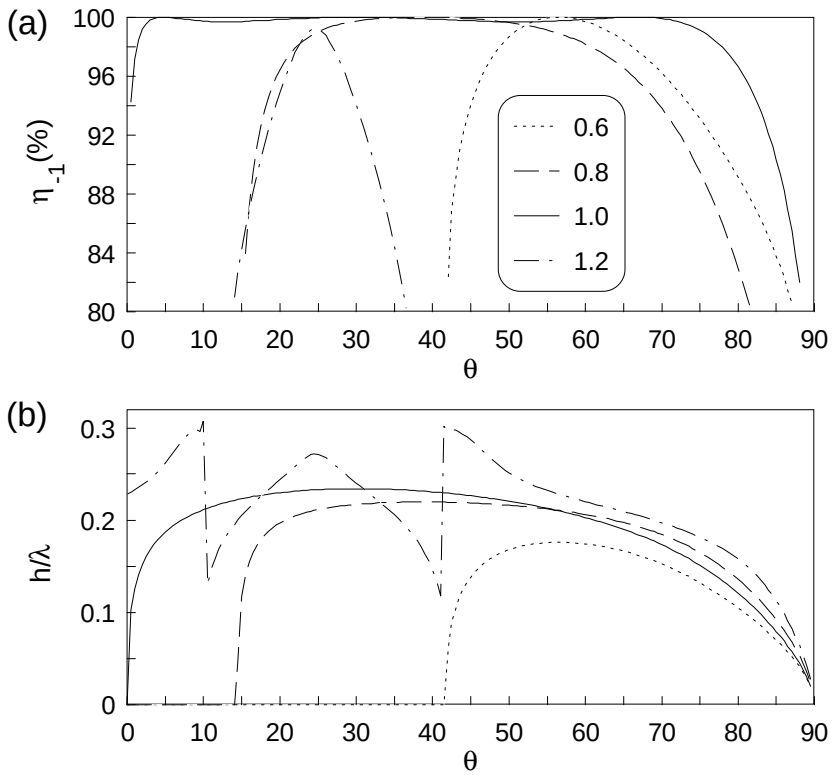

Figure 25: (a) Maximum first-order efficiency as a function of the angle of incidence θ for reflection-type binary high-frequency gratings with aspect ratio $c/d_c = 0.5$ and periods $d/\lambda = 0.6$, 0.8, 1.0, and 1.2. (b) The corresponding optimal relief depth h.

tion of the carrier structure. This puts constraints on the angular width of the signal window.

Polarization-insensitive designs [99] offer an interesting possibility: the solution $\{d_c/\lambda, c/d_c, h/\lambda\} = \{1.0, 0.59, 1.98\}$ gives the efficiencies $\eta_{\mathrm{TE}} = 97.5\%$ and $\eta_{\mathrm{TM}} = 97.9\%$ in transmission mode, whereas 100% efficiency for both states of polarization is obtained with the reflection-type solution $\{d_c/\lambda, c/d_c, h/\lambda\} = \{1.0, 0.715, 0.433\}$. Fabrication tolerances seem feasible for present microfabrication technologies at least for the transmission-type solution.

5.2 Pulse-frequency-modulated elements

A binary high-frequency carrier grating can be modulated to realize continuous phase modulation. This can be achieved by modulating either the pulse width [32–35] or

the pulse frequency [98] of the carrier structure. The latter approach is illustrated in Fig. 26: a steep linear carrier phase that corresponds to the unmodulated carrier grating is added to the ideal phase profile designed by paraxial scalar theory, and the resulting phase profile is then binarized (modulo 2π). This results in pulse-frequency modulation of the carrier grating; i.e., the local period of the carrier structure is slightly modulated but the local aspect ratio is almost unaffected. If the phase modulation varies slowly compared with the carrier phase, the transverse feature sizes remain practically constant and pulse-width modulation becomes negligible, leaving pulse-position modulation dominant; the effect can then be interpreted with the use of the detour-phase principle [19,79]. The first diffraction order is split through the modulation into a set of diffraction orders whose intensity distribution should be asymptotically (in the paraxial limit) equal to the spectrum produced by the ideal phase function. In particular, the diffraction efficiency should converge towards the paraxial prediction multiplied by the Bragg efficiency η_{-1} of the carrier grating.

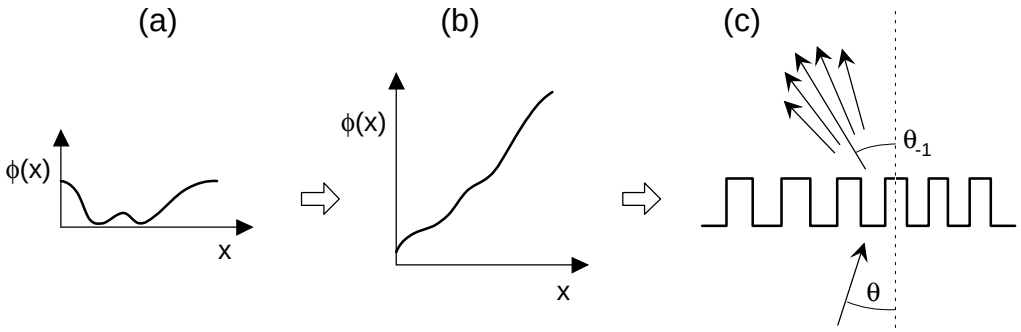

Figure 26: Synthesis of binary pulse-frequency-modulated carrier grating structures: (a) ideal paraxial phase profile, (b) addition of a linear carrier phase, (c) modulo-2π binarization of the phase profile.

We concentrate here on array-illuminator elements that generate 4, 8, or 16 equally intense orders with an efficiency above 90% and with an array uniformity better than 1%. We construct the pulse-frequency-modulated binary structures using carrier period $d_c = \lambda$. To demonstrate the validity of the pulse-frequency-modulation approach, the amplitude and the phase of the transmission function (excluding the evanescent orders) for a 1-to-8 array generator with $d = 50\lambda$ are shown in Fig. 27; one period of the element consists now of 50 modulated carrier periods. When the effect of the carrier is eliminated, the phase profile varies rather smoothly, following closely to the ideal continuous phase function. The slight amplitude oscillations are likely to deteriorate the performance of the element; the fidelity is fairly good though with $\eta = 91\%$ and

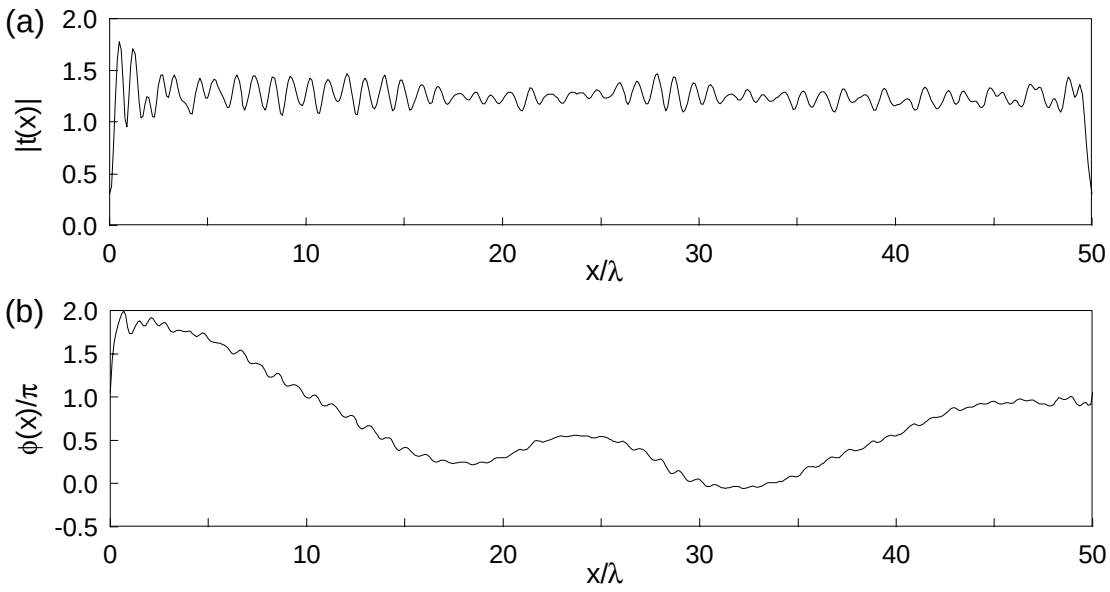

Figure 27: (a) Amplitude and (b) phase of the transmission function (with carrier removed) for a binary high-frequency-carrier 1-to-8 array illuminator with carrier period $d_c = \lambda$ and period $d = 50\lambda$.

$E = 11\%$.

The convergence towards the paraxial predictions as the number of carrier periods is increased is studied in Fig. 28. The normalized diffraction efficiencies $\eta/(\eta_c\eta_{-1})$, where η_c is the paraxial efficiency of the continuous-profile solution, and the array uniformity errors E for transmission-type and reflection-type array generators are plotted as a function of the normalized period $d/N_{\max} = Ld_c/N_{\max}$ (where $N_{\max} = N_s/2$) similarly to Section 3.2 (cf. Figs. 6 and 8). In addition, transmission-type elements based on pulse-width-modulation of a zeroth-order carrier grating with $d_c = 0.4\lambda$ [see Fig. 1(d) of Paper VI] are analyzed for comparison; the efficiencies are now normalized with η_c and the zeroth-order efficiency η_0 averaged over the employed groove widths. The advantage of the pulse-width-modulation scheme is its on-axis reconstruction geometry; on the other hand, it involves deeper grooves and smaller transverse features (we chose $h = 3\lambda$ and $c_{\min} = d_c/6$).

The reflection-type elements show the best convergence: the fidelity reduces only below a well-defined transition point at $d \approx 10N_{\max}\lambda = 5N_s\lambda$ (almost identical behavior to the transmission-type EOM gratings analyzed in Section 3.2). There are no essential differences between the two coding methods in transmission mode. When a longer carrier period $d_c = 0.8\lambda$ is chosen for pulse-width modulation, however, the efficiencies are reduced by $\sim 10\%$ because of the appearance of the reflected orders

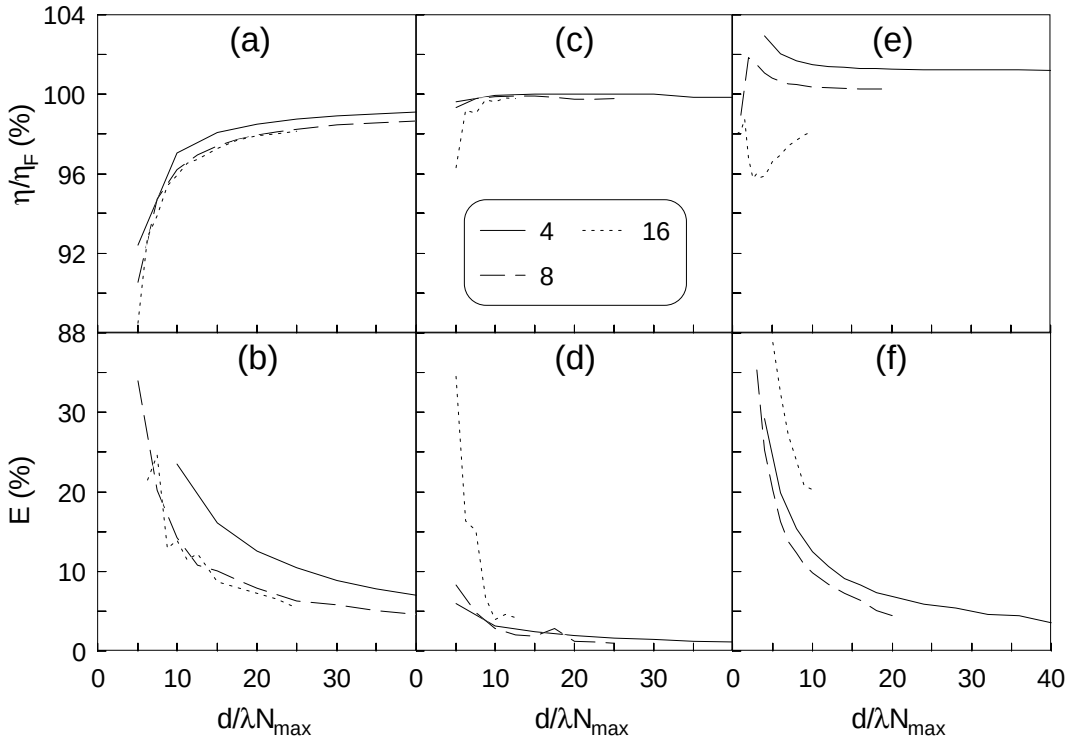

Figure 28: (a) Normalized diffraction efficiencies and (b) array uniformity errors plotted as a function of the normalized period $d/N_{\max}$ for transmission-type pulse-frequency-modulated binary array illuminators with fan-out to 4, 8, and 16. (c) – (d) Results for reflection-type perfectly conducting elements. (e) – (f) Results for transmission-type pulse-width-modulated elements.

± 1. The overall performance is somewhat better than for the conventional binary and multilevel elements that may contain very small features.

6 Conclusions

In this thesis electromagnetic diffraction theory has been used to analyze diffractive optical elements with complicated periodic structures. A wide range of Fourier-type and Fresnel-type elements have been covered from the resonance domain to the paraxial domain with periods as high as 200λ. For this purpose several numerical algorithms have been developed that allow the analysis of dielectric, metallic, and perfectly conducting elements with two-dimensional profiles, as well as dielectric elements with three-dimensional profiles.

We have first considered Fourier-type array illuminators with two-level and multilevel profiles designed by paraxial scalar theory (Fourier optics). The predicted performance is achieved in the paraxial limit ($d \to \infty$), but the fidelity of the elements is severely deteriorated as the non-paraxial domain is entered, resulting in a total failure in the resonance domain. We have found the designs where the even-numbered orders are suppressed (EOM gratings) most preferable in view of their tolerance to resonance effects and fabrication errors.

The strong volume and polarization effects associated with the resonance domain have been utilized to synthesize high-efficiency fan-out elements and star-couplers with a signal window extending over the whole half-space, as well as novel polarization-sensitive elements that lack conventional counterparts. These designs include binary dielectric and perfectly conducting elements with two-dimensional lamellar profiles, and binary dielectric elements with three-dimensional circular, rectangular, and trapezoidal features.

We have presented a new method for synthesizing Fresnel-type diffractive elements with increased efficiency: we have treated their sawtooth-like local groove structures as multilevel staircase gratings and eliminated successfully the drop of the first-order efficiency in the resonance domain through a rigorous optimization of the grating profile. We have then enhanced the operation of microlens arrays by constructing the lens profile using optimized local groove structures with aberration correction by the detour-phase principle. The increase of the focal peak intensity is considerable ($> 30\%$) in particular for high numerical apertures (faster than $F : 1$). Furthermore, we have investigated the Talbot effect and the self-imaging of electromagnetic fields upon propagation. The grating profiles themselves do not self-image even approximately in the resonance domain; the concept of self-imaging must therefore be restricted to the propagating part of the diffracted field. We have also shown that exact self-imaging is

possible under certain conditions.

In the final part of the thesis we have studied diffractive elements realized as binary pulse-frequency-modulated high-frequency gratings. The continuous phase profile of the diffractive element may be designed with the use of paraxial scalar theory and transformed into a pulse-frequency-modulated binary surface-relief profile, the groove structure of which is optimized rigorously to give nearly 100% first-order efficiency. No explicit quantization is involved; therefore the only factor that reduces the ideal diffraction efficiency is the Bragg efficiency of the carrier grating. We have applied this scheme to construct array illuminator elements with $\sim 90\%$ efficiencies. Their performance in the non-paraxial domain is comparable to the results of another synthesis method, the pulse-width-modulation of a subwavelength-period zeroth-order grating, and is in general better than for ordinary binary and multilevel elements.

In summary, the methods and the results presented in this thesis prove the versatility of the rigorous algorithms based on electromagnetic diffraction theory and show their benefits in a wide range of applications of diffractive optics. Among the most important scientific contributions are the resonance-domain beam splitter designs, which have raised international interest and have found a variety of potential and practical applications in the optical information processing systems being developed in Europe. Other major advances are the rigorous synthesis method for Fresnel-domain diffractive elements, as well as the pulse-frequency-modulation scheme, which has also been demonstrated experimentally.

Our near-future prospects include the implementation of other numerical methods to permit accurate analysis of metallic highly-conducting gratings also in TM polarization. We also plan to extend the modal method for perfectly conducting gratings to three-dimensional profiles. On the other hand, our present methods have still plenty of promising applications: we intend to investigate, e.g., guided-mode resonance filters.

References

[1] J. W. Goodman, *Introduction to Fourier Optics* (McGraw-Hill, San Francisco, 1968).

[2] Lord Rayleigh, "On the dynamical theory of gratings", *Proc. Roy. Soc.* **A79**, 399–416 (1907).

[3] E. W. Palmer, M. C. Hutley, A. Franks, J. F. Verrill, and B. Gale, "Diffraction gratings", *Rep. Prog. Phys.* **38**, 975–1048 (1975).

[4] R. Petit, ed., *Electromagnetic Theory of Gratings* (Springer-Verlag, Berlin, 1980).

[5] R. W. Wood, "On a remarkable case of uneven distribution of light in a diffraction grating spectrum", *Phil. Mag.* **4**, 396–408 (1902).

[6] A. Hessel and A. A. Oliner, "A new theory of Wood's anomalies on optical gratings", *Appl. Opt.* **4**, 1275–1297 (1965).

[7] M. Nevière, "The homogeneous problem", in *Electromagnetic Theory of Gratings*, R. Petit, ed. (Springer-Verlag, Berlin, 1980), pp. 123–157.

[8] J. R. Andrewartha, J. R. Fox, and I. J. Wilson, "Resonance anomalies in the lamellar grating", *Opt. Acta* **26**, 69–89 (1979).

[9] T. Tamir, ed., *Integrated optics*, Vol. 41 of *Topics in Applied Physics* (Springer-Verlag, Berlin, 1979).

[10] M. C. Hutley and D. Maystre, "Total absorption of light by a diffraction grating", *Opt. Commun.* **19**, 431–436 (1976).

[11] L. Mashev and E. Popov, "Anomalies of metallic diffraction gratings", *J. Opt. Soc. Am. A* **6**, 1561–1567 (1989).

[12] R. Magnusson and S. S. Wang, "New principle for optical filters", *Appl. Phys. Lett.* **61**, 1022–1024 (1992).

[13] S. S. Wang and R. Magnusson, "Theory and applications for guided-mode resonance filters", *Appl. Opt.* **32**, 2606–2613 (1993).

[14] D. Maystre, "Rigorous vector theories of diffraction gratings", in *Progress in Optics*, E. Wolf, ed. (North-Holland, Amsterdam, 1984), Vol. XXI, pp. 1–67.

[15] W. H. F. Talbot, "Facts relating to optical science, No. IV", *Philos. Mag.* **9**, 401–407 (1836).

[16] K. Miyamoto, "The phase Fresnel lens", *J. Opt. Soc. Am.* **51**, 17–20 (1961).

[17] D. Gabor, "A new microscopic principle", *Nature* **161**, 777–778 (1948).

[18] E. N. Leith and J. Upatnieks, "Reconstructed wavefronts and communication theory", *J. Opt. Soc. Am.* **52**, 1123–1130 (1962).

[19] A. W. Lohmann and D. P. Paris, "Binary Fraunhofer holograms, generated by computer", *Appl. Opt.* **6**, 1739–1748 (1967).

[20] W.-H. Lee, "Computer-generated holograms: Techniques and applications", in *Progress in Optics*, E. Wolf, ed. (North-Holland, Amsterdam, 1978), Vol. XVI, pp. 121–231.

[21] W. J. Dallas, "Computer-generated holograms", in *The Computer in Optical Research: Methods and Applications*, B. R. Frieden, ed. (Springer-Verlag, Berlin, 1980), Vol. 41 of *Topics in Applied Physics*, pp. 291–366.

[22] O. Bryngdahl and F. Wyrowski, "Digital holography - computer-generated holograms", in *Progress in Optics*, E. Wolf, ed. (North-Holland, Amsterdam, 1990), Vol. XXVIII, pp. 1–86.

[23] F. Wyrowski and O. Bryngdahl, "Digital holography as part of diffractive optics", *Rep. Prog. Phys.* **54**, 1481–1571 (1991).

[24] J. Turunen, F. Wyrowski, and E. Noponen, "Transition from paraxial to nonparaxial domain in diffractive optics", in *Diffractive and Holographic Optics Technology*, I. Cindrich and S. H. Lee, eds., Proc. SPIE **2152** (in press, 1994).

[25] J. Turunen, E. Noponen, and F. Wyrowski, "Diffractive optics beyond the paraxial domain", in *Diffractive Optics: Design, Fabrication and Applications*, OSA Topical Meeting, June 6–8, 1994, Rochester, USA, in press.

[26] T. K. Gaylord, W. E. Baird, and M. G. Moharam, "Zero-reflectivity high spatial-frequency rectangular-groove dielectric surface-relief gratings", *Appl. Opt.* **25**, 4562–4567 (1986).

[27] Y. Ono, Y. Kimura, Y. Ohta, and N. Nishida, "Antireflection effect in ultrahigh spatial-frequency holographic relief gratings", *Appl. Opt.* **26**, 1142–1146 (1987).

[28] E. N. Glytsis and T. K. Gaylord, "High-spatial-frequency binary and multilevel stairstep gratings: polarization-selective mirrors and broadband antireflection surfaces", *Appl. Opt.* **31**, 4459–4470 (1992).

[29] D. H. Raguin and G. M. Morris, "Analysis of antireflection-structured surfaces with continuous one-dimensional surface profiles", *Appl. Opt.* **32**, 2582–2598 (1993).

[30] R. C. Enger and S. K. Case, "Optical elements with ultrahigh spatial-frequency surface corrugations", *Appl. Opt.* **22**, 3220–3228 (1983).

[31] L. H. Cescato, E. Gluch, and N. Streibl, "Holographic quarterwave plates", *Appl. Opt.* **29**, 3286–3290 (1990).

[32] W. Stork, N. Streibl, H. Haidner, and P. Kipfer, "Artificial distributed-index media fabricated by zero-order gratings", *Opt. Lett.* **16**, 1921–1923 (1991).

[33] H. Haidner, P. Kipfer, W. Stork, and N. Streibl, "Zero-order gratings used as an artificial distributed index medium", *Optik* **89**, 107–112 (1992).

[34] H. Haidner, J. T. Sheridan, J. Schwider, and N. Streibl, "Design of blazed grating consisting of metallic subwavelength binary grooves", *Opt. Commun.* **98**, 5–10 (1993).

[35] M. W. Farn, "Binary gratings with increased efficiency", *Appl. Opt.* **31**, 4453–4458 (1992).

[36] A. Vasara, E. Noponen, J. Turunen, J. M. Miller, and M. R. Taghizadeh, "Rigorous diffraction analysis of Dammann gratings", *Opt. Commun.* **81**, 337–342 (1991).

[37] J. M. Miller, M. R. Taghizadeh, J. Turunen, N. Ross, E. Noponen, and A. Vasara, "Kinoform array illuminators in fused silica", *J. Mod. Opt.* **40**, 723–732 (1993).

[38] R. C. McPhedran and D. Maystre, "On the theory and solar application of inductive grids", *Appl. Phys.* **14**, 1–20 (1977).

[39] P. Vincent, "A finite-difference method for dielectric and conducting crossed gratings", *Opt. Commun.* **26**, 293–296 (1978).

[40] G. H. Derrick, R. C. McPhedran, D. Maystre, and M. Nevière, "Crossed gratings: a theory and its applications", *Appl. Phys.* **18**, 39–52 (1979).

[41] R. C. McPhedran, G. H. Derrick, and L. C. Botten, "Theory of crossed gratings", in *Electromagnetic Theory of Gratings*, R. Petit, ed. (Springer-Verlag, Berlin, 1980), pp. 227–276.

[42] M. G. Moharam, "Coupled-wave analysis of two-dimensional dielectric gratings", in *Holographic Optics: Design and Applications*, I. Cindrich, ed., Proc. SPIE **883**, 8–11 (1988).

[43] S. T. Han, Y.-L. Tsao, R. M. Walser, and M. F. Becker, "Electromagnetic scattering of two-dimensional surface-relief dielectric gratings", *Appl. Opt.* **31**, 2343–2352 (1992).

[44] R. Bräuer and O. Bryngdahl, "Electromagnetic diffraction analysis of two-dimensional gratings", *Opt. Commun.* **100**, 1–5 (1993).

[45] J. R. Reitz, F. J. Milford, and R. W. Christy, *Foundations of Electromagnetic Theory* (Addison-Wesley, 3. edition, 1979).

[46] C. B. Burckhardt, "Diffraction of a plane wave at a sinusoidally stratified dielectric grating", *J. Opt. Soc. Am.* **56**, 1502–1509 (1966).

[47] F. G. Kaspar, "Diffraction by thick, periodically stratified gratings with complex dielectric constant", *J. Opt. Soc. Am.* **63**, 37–45 (1973).

[48] K. Knop, "Rigorous diffraction theory for transmission phase gratings with deep rectangular grooves", *J. Opt. Soc. Am.* **68**, 1206–1210 (1978).

[49] M. G. Moharam and T. K. Gaylord, "Diffraction analysis of dielectric surface-relief gratings", *J. Opt. Soc. Am.* **72**, 1385–1392 (1982).

[50] A. Vasara, E. Noponen, J. Turunen, J. M. Miller, M. R. Taghizadeh, and J. Tuovinen, “Rigorous diffraction theory of binary optical interconnects”, in *Holographic Optics III: Principles and Applications*, G. M. Morris, ed., Proc. SPIE **1507**, 224–238 (1991).

[51] International Business Machines Corporation, *Engineering and Scientific Subroutine Library Release 4: Guide and Reference* (5. edition, 1990).

[52] D. Maystre and R. Petit, “Diffraction par un reseau lamellaire infinement conducteur”, *Opt. Commun.* **5**, 90–93 (1972).

[53] L. C. Botten and R. C. McPhedran, “Completeness and modal expansion methods in diffraction theory”, *Opt. Acta* **32**, 1479–1488 (1985).

[54] J. M. Miller, J. Turunen, M. R. Taghizadeh, A. Vasara, and E. Noponen, “Rigorous modal theory for perfectly conducting lamellar gratings”, in *Third International Conference on Holographic Systems, Components, and Applications*, IEE Conference Publication **342**, 99–102 (1991).

[55] A. Vasara, M. R. Taghizadeh, J. Turunen, J. Westerholm, E. Noponen, H. Ichikawa, J. M. Miller, T. Jaakkola, and S. Kuisma, “Binary surface-relief gratings for array illumination in digital optics”, *Appl. Opt.* **31**, 3320–3336 (1992).

[56] T. K. Gaylord and M. G. Moharam, “Analysis and applications of optical diffraction by gratings”, *Proc. IEEE* **73**, 894–937 (1985).

[57] M. G. Moharam and T. K. Gaylord, “Rigorous coupled-wave analysis of planar-grating diffraction”, *J. Opt. Soc. Am.* **71**, 811–818 (1981).

[58] M. G. Moharam and T. K. Gaylord, “Rigorous coupled-wave analysis of grating diffraction — E-mode polarization and losses”, *J. Opt. Soc. Am.* **73**, 451–455 (1983).

[59] M. G. Moharam and T. K. Gaylord, “Three-dimensional vector coupled-wave analysis of planar-grating diffraction”, *J. Opt. Soc. Am.* **73**, 1105–1112 (1983).

[60] K. Rokushima and J. Yamakita, “Analysis of anisotropic dielectric gratings”, *J. Opt. Soc. Am.* **73**, 901–908 (1983).

[61] R. Magnusson and T. K. Gaylord, “Equivalence of multiwave coupled-wave theory and modal theory for periodic-media diffraction”, *J. Opt. Soc. Am.* **68**, 1777–1779 (1978).

[62] J. T. Sheridan and C. J. R. Sheppard, “An examination of the theories for the calculation of diffraction by square wave gratings: 1. Thickness and period variations for normal incidence”, *Optik* **85**, 25–32 (1990).

[63] J. T. Sheridan and C. J. R. Sheppard, “An examination of the theories for the calculation of diffraction by square wave gratings: 2. Angular variation”, *Optik* **85**, 57–66 (1990).

[64] L. C. Botten, R. C. McPhedran, J. L. Adams, J. R. Andrewartha, and M. S. Craig, "The dielectric lamellar diffraction grating", *Opt. Acta* **28**, 413–428 (1981).

[65] L. C. Botten, R. C. McPhedran, J. L. Adams, J. R. Andrewartha, and M. S. Craig, "The finitely conducting lamellar diffraction grating", *Opt. Acta* **28**, 1087–1102 (1981).

[66] L. C. Botten, R. C. McPhedran, and M. S. Craig, "Highly conducting lamellar diffraction grating", *Opt. Acta* **28**, 1103–1106 (1981).

[67] L. Li and C. W. Haggans, "Convergence of the coupled-wave method for metallic lamellar diffraction gratings", *J. Opt. Soc. Am. A* **10**, 1184–1189 (1993).

[68] H. P. Herzig, M. T. Gale, H. W. Lehmann, and R. Morf, "Diffraction theory", in *Perspectives for Parallel Optical Interconnects*, Ph. Lalanne and P. Chavel, eds. (Springer, Berlin, 1993), pp. 79–85.

[69] D. Maystre, "Integral methods", in *Electromagnetic Theory of Gratings*, R. Petit, ed. (Springer-Verlag, Berlin, 1980), pp. 63–100.

[70] S. Kirkpatrick, C. D. Gelatt, Jr., and M. P. Vecchi, "Optimization by simulated annealing", *Science* **220**, 671–680 (1983).

[71] J. Turunen, A. Vasara, and J. Westerholm, "Kinoform phase relief synthesis: a stochastic method", *Opt. Eng.* **28**, 1162–1167 (1989).

[72] F. Wyrowski, "Diffractive optical elements: iterative calculation of quantized, blazed phase structures", *J. Opt. Soc. Am. A* **7**, 961–969 (1990).

[73] H. Lüpken, T. Peter, F. Wyrowski, and O. Bryngdahl, "Phase synthesis for array illuminator", *Opt. Commun.* **91**, 163–167 (1992).

[74] H. Dammann and K. Görtler, "High-efficiency in-line multiple imaging by means of multiple phase holograms", *Opt. Commun.* **3**, 312–315 (1971).

[75] N. Streibl, K.-H. Brenner, A. Huang, J. Jahns, J. Jewell, A. W. Lohmann, D. A. B. Miller, M. Murdocca, M. E. Prise, and T. Sizer, "Digital optics", *Proc. IEEE* **77**, 1954–1969 (1989).

[76] N. Streibl, "Beam shaping with optical array generators", *J. Mod. Opt.* **36**, 1559–1573 (1990).

[77] S. J. Walker, J. Jahns, L. Li, M. Mansfield, P. Mulgrew, D. M. Tennant, C. W. Roberts, L. C. West, and N. K. Ailawadi, "Design and fabrication of high-efficiency beam splitters and beam deflectors for integrated planar micro-optic systems", *Appl. Opt.* **32**, 2494–2501 (1993).

[78] L. B. Lesem, P. M. Hirsch, and J. A. Jordan, Jr., "The kinoform: a new wavefront reconstruction device", *IBM J. Res. Dev.* **13**, 150–155 (1969).

[79] J. Turunen, J. Fagerholm, A. Vasara, and M. R. Taghizadeh, "Detour-phase kinoform interconnects: the concept and fabrication considerations", *J. Opt. Soc. Am. A* **7**, 1202–1208 (1990).

[80] A. Vasara, J. Turunen, J. Westerholm, and M. R. Taghizadeh, "Stepped-phase kinoforms", in *Optics in Complex Systems*, F. Lanzl, H.-J. Preuss, and G. Weigelt, eds., Proc. SPIE **1319**, 298–299 (1990).

[81] U. Killat, G. Rabe, and W. Rave, "Binary phase gratings for star couplers with high splitting ratio", *Fiber Integr. Opt.* **4**, 159–167 (1982).

[82] P. B. Fischer and S. Y. Chou, "Sub-50 nm high aspect-ratio silicon pillars, ridges, and trenches fabricated using ultrahigh resolution electron beam lithography and reactive ion etching", *Appl. Phys. Lett.* **62**, 1414–1416 (1993).

[83] H. Nishihara and T. Suhara, "Micro Fresnel lenses", in *Progress in Optics*, E. Wolf, ed. (North-Holland, Amsterdam, 1987), Vol. XXIV, pp. 1–40.

[84] P. Beckmann, "Scattering of light by rough surfaces", in *Progress in Optics*, E. Wolf, ed. (North-Holland, Amsterdam, 1967), Vol. VI, pp. 53–69.

[85] N. Streibl, U. Nölscher, J. Jahns, and S. Walker, "Array generation with lenslet arrays", *Appl. Opt.* **30**, 2739–2742 (1991).

[86] M. Haruna, M. Takahashi, K. Wakahayashi, and H. Nishihara, "Laser beam lithographed micro-Fresnel lenses", *Appl. Opt.* **29**, 5120–5126 (1990).

[87] L. d'Auria, J. P. Huignard, A. M. Roy, and E. Spitz, "Photolithographic fabrication of thin film lenses", *Opt. Commun.* **5**, 232–235 (1972).

[88] J. Jahns and S. J. Walker, "Two-dimensional array of diffractive microlenses fabricated by thin film deposition", *Appl. Opt.* **29**, 931–936 (1990).

[89] J. J. Stamnes, *Waves in Focal Regions* (Adam Hilger, Bristol, 1986).

[90] K. Patorski, "The self-imaging phenomenon and its applications", in *Progress in Optics*, E. Wolf, ed. (North-Holland, Amsterdam, 1989), Vol. XXVII, pp. 1–108.

[91] J. T. Winthrop and C. R. Worthington, "Theory of Fresnel images: I", *J. Opt. Soc. Am.* **55**, 373–381 (1965).

[92] W. D. Montgomery, "Self-imaging objects of infinite aperture", *J. Opt. Soc. Am.* **57**, 772–778 (1967).

[93] O. Bryngdahl, "Image formation using self-imaging techniques", *J. Opt. Soc. Am.* **63**, 416–419 (1973).

[94] B. Packross, R. Eschbach, and O. Bryngdahl, "Image synthesis using self-imaging", *Opt. Commun.* **56**, 394–398 (1986).

[95] J. R. Leger and G. J. Swanson, "Efficient array illuminator using binary-optics phase plates at fractional-Talbot planes", *Opt. Lett.* **15**, 288–290 (1990).

[96] A. W. Lohmann, "An array illuminator based on the Talbot-effect", *Optik* **79**, 41–45 (1988).

[97] A. W. Lohmann and J. A. Thomas, "Making an array illuminator based on the Talbot effect", *Appl. Opt.* **29**, 4337–4340 (1990).

[98] J. Turunen, P. Blair, J. M. Miller, M. R. Taghizadeh, and E. Noponen, “Bragg holograms with binary synthetic surface-relief profile”, *Opt. Lett.* **18**, 1022–1024 (1993).

[99] A. Hessel, J. Schmoys, and D. Y. Tseng, “Bragg-angle blazing of diffraction gratings”, *J. Opt. Soc. Am.* **65**, 380–384 (1975).

[100] E. V. Jull, J. W. Heath, and G. R. Ebbeson, “Gratings that diffract all incident energy”, *J. Opt. Soc. Am.* **67**, 557–560 (1977).

[101] L. S. Cheo, J. Schmoys, and A. Hessel, “On simultaneous blazing of triangular groove diffraction gratings”, *J. Opt. Soc. Am.* **67**, 1686–1688 (1977).

[102] E. G. Loewen, M. Nevière, and D. Maystre, “Efficiency optimization of rectangular groove gratings for use in the visible and IR regions (TE)”, *Appl. Opt.* **18**, 2262–2266 (1979).

Abstracts of Publications I–VI

I Resonance-domain diffractive optics covers the region where the characteristic feature sizes in the surface-relief modulation structure of the diffractive optical element are comparable to the wavelength of light; it may be viewed as a bridge between synthetic holography and the electromagnetic theory of diffraction gratings and rough surfaces. We consider the problem of synthesizing, in the framework of the electromagnetic theory, various types of periodic resonance domain diffractive optical elements that utilize several diffraction orders. Parametric optimization is used to design one-to-N fan-out elements, N-to-N star couplers, and polarization-controlled optical beam splitters and switches with close to 100% efficiencies and no undesired diffraction orders in the image half-space. Reflection-type fan-out gratings with six and seven output beams are demonstrated experimentally at $\lambda = 10.6\ \mu$m.

II We extend the rigorous eigenmode theory of binary surface-relief gratings to accommodate three-dimensional-modulation profiles, to formulate a synthesis problem for doubly-periodic resonance-domain diffractive elements, and to demonstrate some of its symmetry properties. Several solutions for multiple beam splitters with $\sim 90\%$ transmission-mode diffraction efficiency are obtained by nonlinear parametric optimization. The polarization sensitivity and the required fabrication accuracy are analyzed for some solutions.

III To maximize the efficiency of dielectric diffractive optical elements, we optimized the local groove shape using the rigorous diffraction theory of multilevel surface-relief gratings.

IV We apply the rigorous electromagnetic grating theory and an electromagnetic wave-propagation model with Kirchhoff boundary conditions to analyze and optimize the performance of arrays of cylindrical dielectric multilevel diffractive lenses. We show that the diffraction efficiency of a high-numerical-aperture lens array can be improved if the surface-relief profile is constructed with the use of rigorously optimized grating groove structures, which differ significantly from a multilevel approximation of a triangular profile.

V Electromagnetic diffraction theory is applied to investigate self-imaging of optical fields transmitted by lamellar diffraction gratings. We consider both conventional and fractional Talbot imaging of metallic Ronchi rulings and dielectric surface-relief gratings. Our rigorous approach takes fully into account diffraction inside the modulated grating structure as well as non-paraxial propagation of the electromagnetic field into the observation plane, and it is valid for any grating period. We also show that, for certain grating periods, the transmitted electromagnetic field self-images exactly, regardless of the grating profile.

VI Using rigorous electromagnetic diffraction theory, we evaluate the potential performance and the limitations of coding diffractive optical elements in the form of a pulse-frequency-modulated carrier grating. This coding scheme employs the first diffraction order of an ultrahigh-frequency binary carrier grating, with a period below 1.5 wavelengths. We establish that the pulse-frequency-modulation structure can be designed with the standard synthesis techniques based on paraxial scalar diffraction theory. However, we had to optimize the groove depth, the aspect ratio, and the carrier period with rigorous electromagnetic theory to achieve close to 100% efficiency and the desired polarization properties. Our method is compared with another recent coding scheme that utilizes the zeroth order of a subwavelength-period pulse-width-modulated binary carrier grating.

Errata of Publications I–VI

The following misprints have been found in Papers I–VI:

- **Paper I:**
  - Equation (26) on p. 1210 should read
    $$t(x) = \begin{cases} \exp(4.39i) & \text{when } x/\lambda \in [0, 0.322) \\ 1 & \text{otherwise} \end{cases}$$
- **Paper III:**
  - P. 5910, line 8 from the bottom of the right-hand column:
    $\ldots h(x) = hx/d \ldots$
  - P. 5911, line 3 of the caption of Fig. 1:
    $\ldots K = 2, 4, 8, 16 \ldots$
  - P. 5911, line 2 from the bottom of the left-hand column:
    $\ldots x_k = kd/4 + \Delta_k$, where Δ_k is $\ldots$
- **Paper V:**
  - P. 133, in the middle of the right-hand column:
    $\ldots \mathbf{E}(x, y, z) = \hat{\mathbf{y}} E_0 \exp(iknz) \ldots$
    $\ldots \mathbf{H}(x, y, z) = \hat{\mathbf{y}} H_0 \exp(iknz) \ldots$
  - Equation (6) on p. 133 should read
    $$t_m = \begin{cases} \left(k^2 - \gamma_m^2\right)^{1/2}, & \text{if } |\gamma_m| \le k \\ i\left(\gamma_m^2 - k^2\right)^{1/2}, & \text{if } |\gamma_m| > k \end{cases}$$